MEASUREMENTS OF MANTLE VELOCITIES OF P WAVES WITH A LARGE ARRAY

Thesis by
Lane R. Johnson

In Partial Fulfillment of the Requirements

For the Degree of
Doctor of Philosophy

California Institute of Technology
Pasadena, California
1966
(Submitted May 10, 1966)

ACKNOWLEDGMENTS

It is a pleasure to acknowledge and thank Drs. Stewart Smith and Don Anderson for the advice, encouragement, and understanding which they have so generously contributed throughout the course of this investigation. Thanks are also extended to Mr. LaszloLenches for his assistance and patience. The support of a National Science Foundation Fellowship for the past three years is appreciated. This research was partially supported by the Advanced Research Projects Agency and was monitored by the Air Force Office of Scientific Research under contract AF 49(638) - 1337.

ABSTRACT

A large array has been used to investigate the P-wave velocity structure of the lower mantle. Linear array processing methods are reviewed and a method of nonlinear processing is presented. Phase velocities, travel times, and relative amplitudes of P waves have been measured with the large array at the Tonto Forest Seismological Observatory in Arizona for 125 earthquakes in the distance range of 30 to 100 degrees. Various models are assumed for the upper 771 km of the mantle and the Wiechert-Herglotz method applied to the phase velocity data to obtain a velocity depth structure for the lower mantle. The phase velocity data indicates the presence of a second-order discontinuity at a depth of 840 km, another at 1150 km, and less pronounced discontinuities at 1320, 1700 and 1950 km. Phase velocities beyond 85 degrees are interpreted in terms of a triplication of the phase velocity curve, and this results in a zone of almost constant velocity between depths of 2670 and 2800 km. Because of the uncertainty in the upper mantle assumptions, a final model cannot be proposed, but it appears that the lower mantle is more complicated than the standard models and there is good evidence for second-order discontinuities below a depth of 1000 km. A tentative lower bound of 2881 km can be placed on the depth to the core. The importance of checking the calculated velocity structure against independently measured travel times is pointed out. Comparisons are also made with observed PcP times and the agreement is good. The method of using measured values of the rate of change of amplitude with distances shows promising results.

TABLE OF CONTENTS

I. INTRODUCTION

A seismometer samples the ground motion as a function of time at a single point in space. A seismic array samples the ground motion as a function of both time and space. An array increases the capability of seismic recording from one to a possible four dimensions. This thesis will be confined to the study of two-dimensional arrays for which case the ground motion is sampled in three dimensions, one in time and two in space.

Arrays and array processing are not new to seismology. Early seismologists were well aware of the necessity for recording a seismic disturbance in both space and time. The seismological observatories which were located throughout the world formed their array which they processed by reading the station bulletins and seismological summaries. The networks of stations which were established by some observatories formed arrays of smaller dimensions. Earthquakes cannot be located without some form of array processing. More recently, the measurements of surface wave phase velocities and studies of focal mechanisms have depended greatly upon the array concept. The particular noise problems of exploration geophysics led quite naturally to the use of arrays and the techniques for the design and processing of arrays have been highly developed in that area of geophysics.

In spite of the fact that the array concept had long been a basic part of seismology, the particular types of arrays and array processing with which this thesis is concerned have been developed only in the past decade. As a result of the nuclear test ban negotiations which began in 1958 the VELA UNIFORM program was set up under the direction of the Advanced Research Projects Agency (ARPA) in

1960. Under this program six seismic arrays were constructed in the continental United States. Although the impetus for this emphasis on seismic arrays was due to the nuclear surveyance problem, their implementation was greatly facilitated by technological developments in the fields of data handling and also by the increased availability of large digital computers.

The basic purpose of the arrays constructed under the VELA UNIFORM program was to increase the signal to noise ratio. As a result, the magnitude threshold of detectable events was lowered and a better approximation to the actual signal obtained so that identification criteria could be applied with more confidence. These objectives of the program are reflected in certain common characteristics of the arrays. All are designed for the study of teleseisms. Site locations with low ambient noise levels have been chosen. Since the signal being studied must retain a high degree of coherence across the entire array, the size of such an array is limited. At the same time the array dimensions should be of the order of one wavelength of the signal; further increases in size give an array better azimuthal resolution. The requirements for constant surveyance have dictated that the data be recorded at a central point in parallel channel form and that at least some of the array processing be in real time. The density of the array is determined by balancing efficiency against cost.

Although the two array functions of detection and identification are aimed at the study of the source, such operations cannot be carried out without adequate knowledge of the propagation path. Furthermore, the arrays themselves are a powerful tool for increasing this knowledge. Thus a third objective of the array program has been a comprehensive study of the elastic properties

of the earth. The experimental results of this report are confined to this third area, although some of the techniques presented are equally applicable to the other two.

The literature pertaining to the design and use of arrays is voluminous and spans many fields such as radar, radio astronomy, accoustics, antenna theory, information theory, and data processing in addition to geophysics. The references of this paper are mainly from the geophysical literature; more comprehensive bibliographies can be found in the Texas Instruments report (1961) and Birtill and Whiteway (1965).

The best known properties of the mantle of the earth are the seismic velocities obtained from the study of travel time curves. The method of obtaining these data has changed very little in the past fifty years. Improvements have been mainly in the quality of the data and the removal of systematic errors. The raw data are the travel times from earthquakes. The method of analysis consists of plotting travel time versus epicentral distance, smoothing the data and fitting it with a curve, estimating the apparent velocity which is the first derivative of the curve, and integrating the apparent velocity by the Wiechert-Herglotz method to obtain the velocity in the earth as a function of depth. Scatter in the data may be introduced by errors in the determination of the hypocenter and origin time, by the failure to properly account for the variations in the crust and upper mantle structure at both the source and receiver, or by the misreading of the first motion on the seismogram. Valuable information may also be lost when scatter of this type is removed by smoothing.

An array, which can be used to measure apparent velocities relatively directly, has an attractive potential in that the measurements are not measurements of absolute time and are thus free from

many sources of error. The determination of a more accurate phase velocity curve with an array may reveal features which had previously been lost in the process of smoothing and differentiation. This reasoning provides the motivation for the present project.

Amplitudes of the seismic waves have also been considered. Gutenberg has shown that such data are a very useful aid to the interpretation of the travel time data. The question of whether an array with calibrated standard instruments can provide meaningful information about the variation of amplitude with distance has been investigated.

As indicated by the title, this thesis concerns itself with the presentation and interpretation of experimental data on the velocity distribution in the earth's mantle, which were obtained from an analysis of teleseismic P waves recorded on a large array. Following this introduction some of the definitions and conventions necessary for a discussion of array processing are presented in Section II. Section III is a brief review of linear methods for processing seismic arrays. Section IV contains one example of nonlinear processing. Section V is a practical application of array techniques to a specific array at the Tonto Forest Seismological Observatory in central Arizona. In Section VI the experimental results are presented along with the details of analysis and interpretation. Section VII is a summary.

II. FREQUENCY-WAVENUMBER REPRESENTATION OF SEISMIC WAVES

A. Frequency-Wavenumber Space

To an observer confined to the surface of the earth a seismic wave can be characterized by its frequency f and its horizontal phase velocity $\vec{C}$. Equivalent to $\vec{C}$ is the wavenumber vector

$$\vec{k} = \frac{f\vec{C}}{|\vec{C}|^2} \qquad (II-1)$$

which is a vector parallel to the direction of propagation with a magnitude equal to the inverse of the wavelength. Letting k_x and k_y be the orthogonal projections of $\vec{k}$, we see that a monochromatic plane wave propagating with a constant phase velocity is uniquely represented by a single point $G(f, k_x, k_y)$ in a three-dimensional frequency-wavenumber space. With this point we associate a power density function $G(f, \vec{k})$ which is equal to the square of the amplitude of the plane wave. The above description is summarized by saying that the monochromatic plane wave

$$Z(t, \vec{X}) = A_o \exp\left[i2\pi f_o \left(t - \frac{\vec{X} \cdot \vec{C}_o}{|\vec{C}_o|^2} \right) \right] \qquad (II-2)$$

is represented in frequency-wavenumber space by the density function

$$G(f, \vec{k}) = A_o^* A_o \, \delta(f - f_o) \, \delta\left(\vec{k} - \frac{f\vec{C}_o}{|\vec{C}_o|^2}\right) \qquad (II-3)$$

where the * denotes the complex conjugate and the δ denotes a delta function. In such a representation the non-dispersive broad-band seismic pulse

$$Z(t, \vec{X}) = \int_{-\infty}^{\infty} A(f) \exp\left[i2\pi f\left(t - \frac{\vec{x} \cdot \vec{C}_o}{|\vec{C}_o|^2}\right)\right] df \qquad (II-4)$$

becomes

$$G(f, \vec{k}) = A(f)^* A(f)\ \delta\left(\vec{k} - \frac{f\vec{C}_o}{|\vec{C}_o|^2}\right) \qquad (II-5)$$

which is just a straight line through the origin with a slope equal to C_o. A dispersive pulse would be represented as a curved line in $f - \vec{k}$ space. This representation of seismic waves in $f - \vec{k}$ space is particularly well suited to the description of seismic signals or noise which are known only in a statistical sense. In this case $G(f, \vec{k})$ is defined over a volume of $f - \vec{k}$ space and can be thought of as a type of probability density function.

B. Space and Time Correlations

Consider the case where the plane wave of equation (II-2) is observed at two different locations separated by the vector $\Delta\vec{x}$. Then the cross correlation between the ground motions observed at the two locations is given by

$$\psi(\tau, \Delta\vec{x}) = \lim_{T \to \infty} \frac{1}{2T} \int_{-T}^{T} Z(t, \vec{X})^* \, Z(t + \tau, \vec{X} + \Delta\vec{x}) \, dt$$

$$= \lim_{T \to \infty} \frac{1}{2T} \int_{-T}^{T} A(f)^* \exp[-i2\pi f_o (t - \frac{\vec{X} \cdot \vec{C}_o}{|\vec{C}_o|^2})] A(f) \exp[i2\pi f_o (t+\tau - \frac{(\vec{X}+\Delta\vec{x}) \cdot \vec{C}_o}{|\vec{C}_o|^2})] dt$$

$$= A(f)^* A(f) \exp[i2\pi f_o (\tau - \frac{\Delta\vec{x} \cdot \vec{C}_o}{|\vec{C}_o|^2})] \qquad \text{(II-6)}$$

The three-dimensional Fourier transform of $\psi(\tau, \Delta\vec{x})$ is

$$\int_{-\infty}^{\infty}\int\int \psi(\tau, \Delta\vec{x}) \exp[-i2\pi(f\tau - \vec{k} \cdot \Delta\vec{x})] \, d\tau d\Delta\vec{x}$$

$$= \int_{-\infty}^{\infty}\int\int A(f)^* A(f) \exp[i2\pi f_o (\tau - \frac{\Delta\vec{x} \cdot \vec{C}_o}{|\vec{C}_o|^2})] \exp[-i2\pi(f\tau - \vec{k} \cdot \Delta\vec{x})] \, d\tau d\Delta\vec{x}$$

$$= A(f)^* A(f) \, \delta(f - f_o) \, \delta(\vec{k} - \frac{f\vec{C}_o}{|\vec{C}_o|^2})$$

$$= G(f, \vec{k}) \qquad \text{(II-7)}$$

This points out the general result that the temporal and spatial correlation function $\psi(\tau, \Delta\vec{x})$ and the power density function in $f - \vec{k}$ space, $G(f, \vec{k})$, form a three-dimensional Fourier transform pair. Thus $\psi(\tau, \Delta\vec{x})$ and $G(f, \vec{k})$ are equivalent representations of seismic waves. In working with data which has been sampled in both time and space the mathematics usually become most tractable when expressed in terms of $\psi(\tau, \Delta\vec{x})$, whereas the physical operations involved are most easily visualized in terms of $G(f, \vec{k})$.

C. Intuitive Approach to Array Processing

Let us now use the $f-\vec{k}$ space representation of seismic waves to illustrate an intuitive approach to array processing. Consider the problem where a P wave with a velocity $\vec{C}_P$ arrives at an array at the same time as a Rayleigh wave with a velocity $\vec{C}_R$. We want to separate the P wave 'signal' from the Rayleigh wave 'noise'. Such a situation is illustrated in Figure (1-a). Assume we have the time traces from a dense horizontal array of vertical seismometers.

The effect of band-pass filtering is shown in Figure (1-b). The pass band is a slice of $f-\vec{k}$ space parallel to the $\vec{k}$ plane. Such filtering includes some of the noise, and also leaves out some of the signal so that distortion results.

The effect of summing all of the seismometers is shown in Figure (1-c). The pass band is a cylinder parallel to the f axis. Again note that the pass band includes some of the noise and only part of the signal.

The effect of shifting the seismometers in time so as to align the P wave on all of the traces before summing is shown in Figure (1-d). Noise is still included in the pass band but the signal is no longer distorted.

From these simple examples we can intuitively see that a better type of processing would be a combination of the three operations, time shifting, summation, and frequency filtering. A result such as that shown in Figure (1-e) would then be possible. The signal distortion is small and only a small amount of noise is included in the pass band. An even more desirable result, which

could be obtained by applying frequency dependent weighting factors to the channels before summing, is shown in Figure (1-f).

This example shows the potential of array processing as a means of separating in the time domain two waves which are separated in the frequency-wavenumber domain. It also presents an intuitive sketch of a method for achieving this separation. A third result which is implied is that the signal and noise must be separated in $f-\vec{k}$ space if array processing is to be effective. Fortunately, such a situation is very common in seismology where compressional waves, shear waves, and surface waves all travel with different velocities. The situation in other fields, such as radar where all waves have a common velocity, is not so fortunate.

D. The Problems of Aliasing and Resolution

It is well known that for the case of a sampled time series, the resolution of the series is a function of its total length, and aliasing in the frequency domain is controlled by the rate of sampling. Analogous concepts exist for a series which is the result of sampling in space. To illustrate this consider an array of J seismometers where the j-th seismometer is located at $\vec{X}_j$ and its output is given by $Z^j(t)$. The result of summing the outputs of the seismometers is

$$Y(t) = \frac{1}{J} \sum_{j=1}^{J} Z^j(t) \qquad \text{(II-8)}$$

We define the frequency-wavenumber response of an operation upon a sampled time and space function as the ratio of the output to a monochromatic plane wave input

$$A_o \exp[i2\pi f(t - \frac{\vec{X} \cdot \vec{C}_o}{|\vec{C}_o|^2})] \qquad \text{(II-9)}$$

Thus the $f-\vec{k}$ response of the summation operation expressed above is

$$H(f,\vec{k}) = \frac{1}{J}\sum_{j=1}^{J} \exp[-i2\pi\, \vec{k} \cdot \vec{X}_j\ ] \qquad \text{(II-10)}$$

Now consider a linear array with a uniform spacing of $\Delta\vec{x}$ and a total length of $\vec{X}$. In this case it is easy to see that

$$H(f,\vec{k}) = H(f,\vec{k} + \Delta\vec{k}) \qquad \text{(II-11)}$$

whenever

$$\Delta\vec{k} \cdot \Delta\vec{x} = \text{integer} \qquad \text{(II-12)}$$

This is an example of aliasing in the wave number domain as a result of uniform sampling in the spatial domain. Next let the number of elements in the linear array become very large while holding the length $\vec{X}$ constant. In the limit we have

$$H(f,\vec{k}\,) \rightarrow \frac{\sin(\pi\vec{k} \cdot \vec{X})}{\pi\vec{k} \cdot \vec{X}} \qquad \text{(II-13)}$$

This illustrates the point that the resolution or aperture of the array is limited by its maximum dimension. It also illustrates the existence of side lobes. Robinson (1964) has pointed out that for uniform weighting of a linear array, very little improvement in resolution is achieved by using more than 10 elements.

For the more general case of a two-dimensional array, wavenumber aliasing still exists if the seismometers are located on a systematic grid (Burg, 1964), while the aperture and side lobes for a dense packing of elements on a circle of radius X approaches the limit

$$H(f, \vec{k}) \rightarrow J_0(2\pi kX) \qquad (II\text{-}14)$$

Birtill and Whiteway (1965) have plotted the wavenumber responses for a number of different array geometries and the properties of wavenumber aliasing, aperture size, and side lobes are well illustrated. The shape of the aperture and its side lobes can be controlled to a certain degree by weighting the elements of the array before summing and this problem has received considerable attention in the literature.

III. LINEAR ARRAY PROCESSING METHODS

In this section we will give a brief review of some of the linear processing schemes which have been proposed for seismic arrays. None of the results are new.

A. Assumptions about the Signal and Noise

Consider an array of J seismometers spread out on a horizontal plane where the position of the j-th seismometer is given by $\vec{X}_j$. The ground motion which is recorded at the j-th seismometer will be called channel j and denoted by $Z^j(t)$. We will be primarily concerned with the sampled or discrete version of $Z^j(t)$ which we will denote by Z_n^j.

We suppose Z_n^j to be composed of two parts, the signal S_n^j and the noise N_n^j.

$$Z_n^j = S_n^j + N_n^j \qquad \text{(III-1)}$$

where both S_n^j and N_n^j have zero means.

Consider $N^j(t)$ to be a random variable with a probability function $F(N^j(t))$. Thus we can refer to the expectation value of any function of $N^j(t)$ as

$$E[\,H(N^j(t))\,] = \int_{-\infty}^{\infty} H(N^j(\xi))\, F(N^j(\xi))\, d\xi \qquad \text{(III-2)}$$

In most instances the noise will enter into the mathematics in terms of its covariance matrix, whose elements are defined by

$$N_{\psi_{jk}}(m,n) = E[N_m^j \; N_n^k] \tag{III-3}$$

Note that

$$N_{\psi_{jk}}(m,n) = N_{\psi_{kj}}(n,m) \tag{III-4}$$

If we assume that the noise is wide-sense stationary in time we can write

$$N_{\psi_{jk}}(m,n) = N_{\psi_{jk}}(n-m) \tag{III-5}$$

whereas the assumption that the noise is wide-sense stationary in space is implied by

$$N_{\psi_{jk}}(m,n) = N_{\psi}(m,n,\vec{X}_k-\vec{X}_j) \tag{III-6}$$

White noise has the covariance matrix

$$N_{\psi_{jk}}(m,n) = \delta_{mn} \; N_{\psi_{jk}} \tag{III-7}$$

and noise uncorrelated between channels has the covariance matrix

$$N_{\psi_{jk}}(m,n) = \delta_{jk} \; N_{\psi_{jj}}(m,n) \tag{III-8}$$

In certain cases it will be necessary to assume that the signal is also a random variable which is wide-sense stationary in time and has the covariance matrix

$$S_{\psi_{jk}}(n-m) = E[S_m^j \; S_n^k] \tag{III-9}$$

In such cases we will also assume that the signal and noise are uncorrelated, i. e.

$$E[S_m^j \, N_n^k] = 0 \qquad \text{(III-10)}$$

More typically we will assume that the signal is an unknown wave form which is the same on all channels except for a time shift β_j which may be either known or unknown. Thus we have

$$S_n^j = S_{n+\beta_j} \qquad \text{(III-11)}$$

Digital filtering of channel j can be expressed by

$$Y_n^j = \sum_{m=-M}^{M} a_m^j \, Z_{n+m}^j \qquad \text{(III-12)}$$

where the a_m^j are $2M + 1$ filter coefficients. Such a filter has zero phase shift when $a_m^j = a_{-m}^j$. Often it is convenient to shift the channels in time so that a particular plane wave traveling across the array will be aligned on all of the channels. For a wave with velocity $\vec{C}$ the shift for channel j is given by

$$\beta_j = \frac{\vec{X}_j \cdot \vec{C}}{|\vec{C}|^2} \qquad \text{(III-13)}$$

A prime (') will be used to indicate that the operation of time shifting has been performed. Thus the result of time shifting, filtering, and summing J channels will be expressed by

$$Y'_n = \sum_{j=1}^{J} a_m^j \, Z_{n+m}^{j'} = \sum_{j=1}^{J} a_m^j \, Z_{n+m+\beta_j}^{j} \qquad \text{(III-14)}$$

In the case of time shifting, modified covariance matrices will be defined by

$$N_{\psi'_{jk}}(n-m) = N_{\psi_{jk}}(n-m+\beta_k-\beta_j) = E[N^j_{m+\beta_j} N^k_{n+\beta_k}] \qquad \text{(III-15)}$$

$$S_{\psi'_{jk}}(n-m) = S_{\psi_{jk}}(n-m+\beta_k-\beta_j) = E[S^j_{m+\beta_j} S^k_{n+\beta_k}] \qquad \text{(III-16)}$$

With these preliminary assumptions and definitions behind us we can now consider the basic problem of linear array processing: Given the J channels of sampled time data obtained at the locations $\vec{X}_j$, how can they be combined in a linear manner so that the signal is enhanced with respect to the noise in some optimum sense? In the sections that follow four of the main methods of linear processing will be considered: time shift and summation, multichannel Wiener filtering, unbiased minimum variance estimation, and maximum likelihood estimation. Since all of these methods have been described in the literature, the mathematical development of the methods will be only briefly outlined here. We will emphasize the assumptions about the noise and signal upon which each of the methods is based and also the sense in which the output is considered to be optimum. After putting the methods adjacent to each other in a common notation, we will be in a position to compare them and examine their relative merits.

B. A Note on Frequency Filtering

Before proceeding it should be pointed out that in what follows very little attention will be devoted to the matter of simple frequency filtering where such filtering is not unique to the problem of array processing. Thus such things as whitening filters, equilization filters to compensate for differences in channel responses, or narrow band filters to take advantage of frequency separation of signal and noise will not be discussed. However, it should be emphasized that such filtering is important in array processing for the same reasons that it is important in the analysis of a single channel. As long as linear filters are used they can be applied to the individual channels of an array before processing or to the processed output without affecting the basic results of the array processing.

C. Time Shift and Summation

The mathematical basis of this method, the most obvious of the array processing schemes, has been pointed out by Kelly and Levin (1964) and the following is a summary of their results.

Assume that the signal is the same on all of the channels except for an unknown time shift. The processing criterion is that the signal should be a least squares fit to the data.

We want to minimize the expression

$$\sum_{j=1}^{J} \sum_{n=1}^{T} (Z^{j}_{n+\beta_j} - S_n)^2 \qquad \text{(III-17)}$$

where we have taken the time interval of interest as being finite ($n = 1, \ldots, T$), and where β_j is a function of the unknown phase velocity as given in equation (III-13). It can be shown that minimizing the above expression is equivalent to finding the phase velocity $\vec{C}$ which maximizes the sum of the cross correlation functions between the channels

$$\sum_{j,k=1}^{J} \sum_{n=1}^{T} Z^j_{n+\beta_j} Z^k_{n+\beta_k} \qquad \text{(III-18)}$$

Having determined $\vec{C}$, the least squares estimate of the signal is the sum

$$S_n = \frac{1}{J} \sum_{j=1}^{J} Z^j_{n+\beta_j} \qquad \text{(III-19)}$$

The development outlined above is not dependent upon any assumptions about the noise. However, when the noise is random, gaussian, and uncorrelated between channels it increases with summation as $\sqrt{J}$. Since the signal increases as J, the signal to noise ratio increases as $\sqrt{J}$. This is the basis for the familiar statement that the maximum improvement in the signal to noise ratio achieved by the summation of J channels in the presence of uncorrelated noise is $\sqrt{J}$.

D. Multichannel Wiener Filter

Developments of this type of processing in both the time and frequency domain can be found in Burg (1964), the Texas Instruments report (1961), and Kelly (1965). Experimental results are given by Backus, et. al., (1964) and the Texas Instruments report (1961).

Assume that the covariance matrix of the noise is known and is wide-sense stationary in time, that the covariance matrix of the signal is known and is wide-sense stationary in time, and that the signal and noise are uncorrelated. The processing criterion is that the variance of the difference between the array output and the known signal should be a minimum.

After filtering the individual channels with the coefficients a_m^j and summing, the array output is

$$Y_n = \sum_{j=1}^{J} \sum_{m=-n}^{M} a_m^j Z_{n+m}^j \qquad \text{(III-20)}$$

Thus we want to minimize the expression

$$E[(Y_n - S_n^o)^2] \qquad \text{(III-21)}$$

as a function of the filter coefficients a_m^j where we have let S_n^o denote the signal at an arbitrary reference point. It is straightforward to show that minimizing this expression is equivalent to solving the system of $J(2M + 1)$ linear equations of the form

$$\sum_{k=1}^{J} \sum_{n=-M}^{M} a_n^k \left\{ {}^{S}\psi_{jk}(n-m) + {}^{N}\psi_{jk}(n-m) \right\} = {}^{S}\psi_{jo}(m) \quad \begin{pmatrix} j=1,\ldots J \\ m=-M,\ldots M \end{pmatrix} \tag{III-22}$$

for the unknown a_n^k.

E. Unbiased Minimum Variance Estimation

This method is given by Kelly (1965) and the following is essentially a summary of his results. Limited experimental results can be found in the Lincoln Laboratory report (Dec., 1964).

Assume that the covariance matrix of the noise is given and is wide-sense stationary in time. Assume that the signal is the same on all of the channels except for a known time shift. The processing criteria are that the output should be an unbiased estimate of the signal and that the variance of the output should be a minimum.

Time shifting the channels of the array in accordance with the known phase velocity of the signal $\vec{C}$, filtering with the coefficients b_m^j, and summing results in

$$Y'_n = \sum_{j=1}^{J} \sum_{m=-M}^{M} b_m^j \, Z_{n+m}^{j'}$$

$$= \sum_{j=1}^{J} \sum_{m=-M}^{M} b_m^j (S_{n+m} + N_{n+m+\beta_j}^{j}) \tag{III-23}$$

The requirement that the mean of Y'_n be an unbiased estimate of the signal results in a set of $2M + 1$ equations of the form

$$\sum_{j=1}^{J} b_m^j = \delta_m \qquad m = -M, \ldots, M \tag{III-24}$$

The variance of Y'_n is given by

$$E[(Y'_n - S_n)^2] \tag{III-25}$$

If we minimize this as a function of the b_m^j and include the restraints of equation (III-24) via the method of Lagrange multipliers, we arrive at a set of $J(2M + 1)$ equations of the form

$$\sum_{k=1}^{J} \sum_{n=-M}^{M} b_n^k \, {}^{N}\psi'_{jk}(n - m) = -L_m \quad \begin{pmatrix} j = 1, \ldots J \\ m = -M, \ldots M \end{pmatrix} \tag{III-26}$$

where the L_m are the Lagrange multipliers. These equations can be solved for b_n^k in terms of the L_m and then substituted in equation (III-24) to eliminate the L_m. An equivalent procedure is to define

$$b_m^{J+1} = L_m \tag{III-27}$$

$${}^{N}\psi'_{J+1,k}(m - n) = {}^{N}\psi'_{k,J+1}(m - n) = (1 - \delta_{k,J+1})\delta_{m,n}$$

and then we have a set of $(J + 1) \cdot (2M + 1)$ equations of the form

$$\sum_{k=1}^{J+1} \sum_{n=-M}^{M} b_n^k \, {}^{N}\psi'_{jk}(n - m) = \delta_{j,J+1}\delta_{m,o} \quad \begin{pmatrix} j=1, \ldots J+1 \\ m=-M, \ldots, M \end{pmatrix} \tag{III-28}$$

which are to be solved for the filter coefficients b_n^k. Note that the minimum variance of the output which is obtained with these filter coefficients is given by L_o.

F. Maximum Likelihood Estimation

Generalizations of this method for the case of seismic arrays are given by Kelly and Levin (1964) and by Kelly (1965).

Assume that the noise is gaussian with a known covariance function. Assume that the signal is identical on all channels except for an unknown time shift. The processing criterion is that the likelihood ratio, which is the ratio of the probability that the signal is present to the probability that the signal is absent, should be a maximum.

Let all of the channels be of length T (Z_n^j; n = 1, ... T) and for the moment consider them to be lumped into a single random valued vector $\underline{Z}$. Let the inverse of the noise covariance matrix $\underline{N}_{\underline{\psi}}$ be denoted by $\underline{\varphi}$. Then the probability function of the noise is given by

$$F(\underline{N}) = \frac{1}{2\pi|\underline{N}_{\underline{\psi}}|} \exp[-\frac{1}{2}\,\underline{N}\,\underline{\varphi}\,\underline{N}^*] \qquad \text{(III-29)}$$

The likelihood ratio is

$$\mathcal{L} = \frac{F(\underline{N} = \underline{Z} - \underline{S})}{F(\underline{N} = \underline{Z})} \qquad \text{(III-30)}$$

Minimizing this as a function of $\underline{S}$ and reverting to our previous notation we have a set of T equations of the form

$$\sum_{j,k=1}^{J} \sum_{m=1}^{T} \varphi_{jk}(n+\beta_j, m) Z_m^k = \sum_{j,k=1}^{J} \sum_{m=1}^{N} \varphi_{jk}(n+\beta_j, m+\beta_k) S_m^o \quad (n = 1, \ldots T) \qquad \text{(III-31)}$$

where S_m^o is the unknown signal at some arbitrary reference point and where we have tentatively assumed a value for the phase velocity of the signal $\vec{C}$ so that the β_j might be fixed. By solving the above set of equations for many different values of $\vec{C}$ we can maximize the likelihood ratio as a function of both the signal shape and phase velocity.

The maximum likelihood approach is conceptially quite different from the other methods described in this section. Whereas the other methods have as their objective an increase in the signal to noise ratio, the likelihood ratio is a statistic which is formulated as an aid to making a decision. Given a set of data we wish to decide if a signal is present or not. By filtering with the coefficients derived from the above set of equations and then calculating the log likelihood ratio and basing our decision on its value, the probability is a maximum that we will decide a signal is present. Note that we could have formulated the problem to make any of a number of decisions such as the arrival time of the signal, the polarity of the signal, or the time delay between the signal and a similar signal following it. This points out the versatility of the maximum likelihood approach. Cramer (1946, p. 499) shows that under rather broad assumptions a maximum likelihood estimate has minimum variance.

G. Comparison of the Methods

Let us now compare the four methods of linear array processing which have been discussed. First note that the time shift and summation method is the only one of the four which does not depend upon a knowledge of the statistical properties of the noise. This method has a maximum improvement in the signal-to-

noise ratio when the noise is uncorrelated between channels. It can be shown that the other three methods have a minimum improvement in the signal-to-noise ratio when the noise is uncorrelated between channels and that in this case all of the processes are essentially equivalent to the first process of time shift and summation. Thus we conclude that if the noise is uncorrelated between channels, the best linear processor is a simple time shift and summation. Furthermore, if the noise is known to be correlated between channels, we can always do better than the time shift and summation method by using one of the other processes. Henceforth, we will consider only these latter three types of processing: multichannel Wiener filtering, unbiased minimum estimation, and maximum likelihood estimation.

It can be shown that under certain assumptions the outputs of the latter three types of processing are all essentially equivalent. Capon and Greenfield (1965) show that for Gaussian noise the unbiased minimum variance estimation and the maximum likelihood estimation yield identical results. Kelly (1965) has shown that multichannel Wiener filtering is equivalent to unbiased minimum variance estimation followed by a one-channel Wiener filter which takes advantage of any frequency separation of signal and noise. Kelly and Levin (1964) show that multichannel Wiener filtering has the same relationship to maximum likelihood estimation. Thus the differences in these latter three types of processing lie in the ease in which the processes can be synthesized in the time domain and in the facility with which the known properties of the signal and noise can be incorporated in the input data of the process.

The equations for the multichannel Wiener filtering and also the unbiased minimum variance estimation can be solved by inverting a Toeplitz matrix, and an algorithm exists for doing this. However,

the maximum likelihood estimation leads to a more complex set of equations and no convenient algorithm for doing this has yet been presented.

The maximum likelihood estimation does have the advantage that it contains a means of estimating the velocity of the signal c in addition to its shape whereas the other two methods do not explicitly contain such a capability.

The multichannel Wiener filtering formulation differs from the other two methods in that it does not assume that the signal is a plane wave crossing the array with a fixed velocity. Thus it is the only one of the three methods which can be easily adapted to the case of a dispersive signal.

IV. NONLINEAR ARRAY PROCESSING

In the previous section it was pointed out that when the noise is well organized, effective linear filters can be designed to eliminate it. However, when the noise is uncorrelated between channels, the optimum linear filter is a simple time shift and summation. In such a situation nonlinear processing methods are an attractive possibility for attaining greater degrees of separation between the signal and noise.

In this section we will consider one such nonlinear method which has been developed for processing a large array where the separation between seismometers is large compared to the distance over which the noise is correlated. This method is very similar to the one developed by Shimshoni and Smith (1964) and extended by Sax and Mims (1965). Both of these papers are concerned with multicomponent data but this is not crucial to the method.

As is true with most nonlinear processes, rigid theoretical justification is very difficult and we shall rely mostly upon experimental results for justification of this particular method as an effective means of array processing.

A. Design of the Filter

Assume that the various channels of the array have been reduced by linear means to only two channels which we will call Z^1 and Z^2. Assume that each of these channels contains independent, wide-sense stationary, white noise and that each contains an identical broad band signal of duration less than 2T where T is a time parameter. Following the notation developed in Section III we have

$$Z_n^1 = S_n + N_n^1$$

$$Z_n^2 = S_n + N_n^2 \qquad \text{(IV-1)}$$

Consider the correlation function over a window $2T + 1$ as defined by

$$Z^1Z^2{}_{\theta_n}(\tau) = \frac{1}{2T+1} \sum_{m=-T}^{T} Z^1_{n+m} Z^2_{n+m+\tau} \qquad \text{(IV-2)}$$

Stated in terms of the correlation functions, our original assumptions are as follows

$$N^1N^1{}_{\theta_n}(\tau) = N^2N^2{}_{\theta_n}(\tau) = \sigma^2 \delta_\tau$$

$$N^1N^2{}_{\theta_n}(\tau) = N^2N^1{}_{\theta_n}(\tau) = 0 \qquad \text{(IV-3)}$$

$$N^1S_{\theta_n}(\tau) = N^2S_{\theta_n}(\tau) = 0$$

We now define a set of $2W + 1$ filter coefficients as

$$A_n(\tau) = \frac{Z^1Z^2{}_{\theta_n}(\tau) + Z^2Z^1{}_{\theta_n}(\tau)}{Z^1Z^1{}_{\theta_n}(0) + Z^2Z^2{}_{\theta_n}(0)} \qquad \text{(IV-4)}$$

This reduces to

$$A_n(\tau) = \frac{SS_{\theta_n}(\tau)}{\sigma^2 + SS_{\theta_n}(0)} \qquad \text{when S is contained in the interval } (n - T,\ n + T)$$

$$A_n(\tau) = 0 \qquad \text{when S is not contained in the interval } (n - T,\ n + T) \qquad \text{(IV-5)}$$

The output of the process is obtained by convolving $A_n(\tau)$ with the average of Z^1 and Z^2 over a window of length 2W where W is a second time parameter.

$$Y_n = \sum_{\tau=-W}^{W} A_n(\tau) \frac{(Z^1_{n+\tau} + Z^2_{n+\tau})}{2} \qquad \text{(IV-6)}$$

B. The Effects of the Filter Window

The characteristics of this filtering operation are very dependent upon the parameter W. When W is equal to T the frequency response of $A_n(\tau)$ is given by

$$a_n(f) = \frac{S_{u(f)}}{\sigma^2 + S_{u(0)}} \qquad \text{when S is contained in the interval } (n - T,\ n + T)$$

$$a_n(f) = 0 \qquad \text{when S is not contained in the interval } (n - T,\ n + T) \qquad \text{(IV-7)}$$

where $S_{u(f)}$ is the power spectrum of the signal. With this choice of W the filter is equivalent to an amplitude factor which depends upon the signal to noise ratio in series with two matched filters. Such a filter would be very useful in detecting a weak signal but would introduce a considerable amount of signal distortion.

When W is equal to zero the filter reduces to a single amplitude factor.

$$A_o(0) = \frac{S_{u(0)}}{\sigma^2 + S_{u(0)}} \qquad \text{when S is contained in the interval } (n - T,\ n + T)$$

$$A_o(0) = 0 \qquad \text{when S is not contained in the interval } (n - T,\ n + T) \tag{IV-8}$$

This filter acts much like a gate which does not admit pure noise, passes both signal and noise with no attenuation when the signal to noise ratio is large, and passes both signal and noise with increasing amounts of attenuation as the signal to noise ratio decreases. Such a filter would be useful for recovering strong signals with minimum distortion.

On the basis of the behavior of the filter for the limit values of W, it seems intuitively reasonable that as W varies from 0 to T increased detection ability will be gained at the expense of increased signal distortion. Thus it may be possible to find an intermediate value of W which results in a satisfactory compromise between these two factors.

To illustrate the effect of W in a more qualitative manner, consider the example of a signal which is one cycle of a sine wave centered at $n = q$ and having a period of $2Q$

$$S_n = s \sin \frac{\pi n}{Q} \qquad (-Q < n - q < Q)$$

$$S_n = 0 \qquad \text{otherwise} \tag{IV-9}$$

If we assume that the sampling interval is small enough so that sums may be approximated by integrals and chose $T > Q$ then it is easy to show that

$$A_q(\tau) = \frac{\pi Q s^2}{\sigma^2 + \pi Q s^2} \cos \frac{\pi \tau}{Q}\left[\left(1 - \frac{|\tau|}{Q}\right) + \frac{1}{2\pi} \sin\frac{(2\pi|\tau|)}{Q}\right] \quad \text{(IV-10)}$$

The situation which results when the signal is present and the noise is small is shown graphically in Figure (2). The spectrum of the signal is u(f) and the transfer function of the filtering operation is shown for three different values of W.

C. Experimental Results

The foregoing discussion was intended primarily to show the motivation behind this particular approach to nonlinear processing. Several matters such as the nonlinear response of the process, the response when the signal is only partially contained in the correlation window, and the effect of noise have been neglected. These effects are best illustrated by empirical results.

Consider first the inherent nonlinearity of this process. This results from the fact that the process varies with time and at any one instant depends upon the present properties of the signal and noise. The nonlinearity can be examined as a function of the two parameters of the process, the correlation window (2T + 1) and the filter window (2W + 1). The effect of T is shown in Figure (3) which shows the process output for different values of T when the input is a pulse of duration 2Q. The filter parameter W is equal to T/2 in all cases. Figure (4) is a graph showing the same effect. As the amplitude of

the input, the pulse shown in Figure (3), was varied. The peak to peak amplitude of both input and output were measured and their ratio plotted in Figure (4). The amplitude is expressed as a ratio to the full scale output of the fixed point computer on which the analysis was performed. The conclusion is drawn that the process becomes more linear as T increases which is consistent with the obvious limit that the process should be linear for T very large. The increased pulse distortion shown in Figure (3) for the case $T = 3Q/2$ is actually due to the parameter W which is maintained at $T/2$ and thus is larger for the case $T = 3/2\ Q$ than for the case $T = Q$. A factor which is not illustrated here is that the noise energy which enters through the correlation window increases with the window length. For this reason it is usually best to choose the window only slightly greater than the signal duration. The effect of varying the filter window $(2W + 1)$ is shown in Figures (5) and (6) for the case where the input is a pulse and the correlation window is equal to the pulse length. Figure (5) shows that the linearity is essentially independent of the parameter W. Figure (6) shows, however, that the pulse distortion increases as W increases. This distortion results from the fact that filtering is an averaging process which tends to smear out a finite pulse.

On the basis of these results, it has become standard procedure to choose W equal to $T/2$ and $(2T + 1)$ equal to the expected pulse duration when using this particular nonlinear process. Unless stated otherwise, these choices will be assumed in the remainder of this report.

Figure (7) is an attempt to estimate the effect of noise. The first line shows four different amplitudes of the same signal which was added to two samples of seismic noise to form the two inputs Z^1 and Z^2. The fourth line is the result of processing Z^1 and Z^2. Note that the process effectively suppresses the uncorrelated noise when the signal is not present but passes a combination of both signal and noise when the signal is present.

The process described here is a first attempt at designing a nonlinear process for extracting a reasonable facsimile of a signal from uncorrelated noise. Many extensions and improvements are possible. This method consists essentially of using the cross correlation function as a filter. Improvement may be possible by constructing a filter from a function of the cross correlation function such as a weighted average or the logarithm. The use of a tapered cross correlation window may also prove helpful. Even in its present unsophisticated form, the process has been extremely useful in isolating secondary P waves of teleseisms recorded on a large array. Some of the results will be given in Section V.

V. APPLICATIONS TO TFSO

A. The Tonto Forest Seismological Observatory

Operation of the Tonto Forest Seismological Observatory (TFSO) began officially in April of 1963 under the direction of the Air Force Technical Applications Center (AFTAC) as a part of the VELA UNIFORM project. It was designed for use both as a standard seismological observatory and also as a research tool for obtaining data which would be helpful in constructing other arrays. The center of the array is near Payson, Arizona, in central Arizona about 90 miles northeast of Phoenix. One of the reasons for selecting this site was the very low ambient noise level.

The permanent array at TFSO consists of a 3 km 31 element circular array (four concentric circles) of short period vertical instruments and a 10 km 12 element linear cross array of short period vertical instruments. Horizontal instruments have also been installed at alternate sites of the cross array. In addition, several long period and broad band instruments are maintained in a vault. All instruments are connected by cable to a central point where they are recorded on develicorder film and on analog magnetic tape.

B. The Extended Array

In 1965 the array was temporarily extended by the addition of eight Long Range Seismic Measurement (LRSM) mobil vans. Each van had six instruments, three short period and three long period, and at any one time the data of four instruments was telemetered to the array center at TFSO. This report is based on data obtained

from the 12 element array consisting of the four end points of the linear cross array at TFSO and the eight LRSM mobil vans. Hereafter, we will refer to this as the extended linear cross array or simply as the extended array. Site locations for the extended array are given in Table 1 and also shown on the map of Figure (8). The NW-SE leg and the NE-SW leg of the array have maximum dimensions of 325 km and 285 km, respectively, and lie along azimuths of 131 degrees and 41 degrees, respectively. The center of the extended array has been taken to be the site Z21 at TFSO which has latitude 34.29 N and longitude 111.27 W. The short period vertical channel from two of the LRSM mobil vans, JRAZ and WOAZ, actually consists of the sum of a 3.5 km 7 element circular sub-array.

Between the dates of April 15, 1965, and August 31, 1965, the data from the short period vertical instruments of the extended array were recorded on develicorder film and on analog magnetic tape for the use of Cal Tech. The present report is based on the analysis of this block of data. Short period horizontal data were also recorded on analog magnetic tape for about half of this period but these have not been analyzed yet. The data on the magnetic tapes have been processed on the Cal Tech hybrid analog-digital computer which was designed and programmed for handling data of this particular type.

C. Instrument Response

The extended array of short period vertical instruments contains two slightly different seismometers. The four sites at TFSO have Johnson-Matheson seismometers with free periods of 1.25 sec and 0.33 sec galvonometers while the eight LRSM mobil

vans have Benioff seismometers with free periods of 1.0 sec and 0.20 sec galvonometers. The two response curves are shown in Figure (9).

D. Wavenumber Response

An expression for the wavenumber response of an array, which describes the response of a summed array to a plane wave input, has been given in equation (II-10). This response has been calculated for the extended array and contoured in 3 db intervals in Figure (10). The widths of the aperture at the center of the K plane, about 0.0035 km^{-1}, corresponds to roughly the inverse of the maximum dimension of the array. In terms of phase velocity, this means that for a 1 cps wave traveling with a phase velocity of 15 km/sec the sum of the extended array has a potential resolving power of approximately 1 km/sec. Also note that the side lobes are the most pronounced along directions parallel to one of the legs of the array. This is one of the disadvantages of crossed arrays. Birtill and Whiteway (1965) have pointed out that these side lobes are greatly reduced if one considers the correlation between the sums of the two legs of the array.

E. Crustal Structure

In most instances one is interested in the properties of seismic waves as they emerge from the mantle and thus it is desirable to remove the effect of the local crust which separates the mantle and the array. This requires knowledge of the velocity structure of the crust. The Branch of Crustal Studies of the U. S. Geological Survey conducted a seismic refraction survey at TFSO,

which consisted of two reversed profiles that approximately coincided with the two legs of the extended array. Warren, et. al., (1965) have published an abstract of the results and additional unpublished data were supplied by Warren. They found that the Moho was at an almost constant depth of 34 km along the NW-SE leg of the extended array. Along the NE-SW leg the Moho dips to the NE and its depth increases from about 22 km at the SW end of the profile to about 40 km at the NE end. Evidence for an intermediate layer was present but not conclusive, the average crustal velocity was about 6.2 km/sec, and the sub-Moho velocity was 7.85 km/sec. Niazi (1965) found similar results from a study of teleseisms recorded on the linear cross array at TFSO. He suggested that the dip of the Moho may be as great as 8 degrees to the NE near the center of the array.

Gravity data (Biehler, unpublished map, 1964) were also used to help determine the crustal structure. These data suggest a general thickening of the crust in a NE direction. They also indicate that the structure is roughly two-dimensional with the axis of uniformity in a NW-SE direction. The observed data along the NE-SW leg of the extended array is plotted in Figure (11). Also shown are two models of the crustal structure along this leg and the theoretical gravity anomalies for such structures. Densities were derived from the velocities by an empirical relation given by Talwani, et. al., (1959). The first model has a crust with a uniform velocity of 6.2 km/sec and a depth determined from the seismic refraction results. In the second model the crust has been modified so as to approximate a latteral gradient in the average crustal velocity.

The fact that the second model results in a much better fit to the observed gravity data is regarded as evidence that the average velocity increases in a NE direction. However, from these results it is not possible to determine if the velocity gradient is actually in the crust as shown or in the upper part of the mantle. For the determination of the delay of teleseismic waves, such a distinction is not of great importance.

Press and Biehler (1964) have shown that it is very reasonable to assume a correlation between the gravity anomaly and the delay of seismic waves. Two other studies of teleseismic time anomalies for the extended array (Lincoln Laboratory Report, 1965; Dean, 1965) have both indicated a time anomaly, approximately -0.5 sec, for the array site farthest to the NE, NLAZ. Assuming a lateral gradient in the crustal velocity helps to explain this anomaly.

On the basis of these data and arguments, a crustal model was assumed for each site of the extended array. Such models are given in Table 2. The crustal velocity is an average one. Decomposing the crust into layers of differing velocities would perhaps be a better approximation to the geologic situation but simple calculations show that it would have a very small effect on the delay time of teleseismic waves. The inclusion of a dipping boundary in the crustal models means that for a particular site, the time delay of a seismic body wave has an azimuthal dependence. For a dip of 5 degrees and a phase velocity of 15 km/sec this effect amounts to $\pm$ 0.1 sec.

F. Measurement of Relative Arrival Times

Given the geometry of an array and the crustal structure underlying it, Tables 1 and 2, it is now possible to calculate the relative arrival times at the various array sites as a function of the phase velocity and azimuth of the incident seismic wave. Assume that below an elevation E_o the velocity is a function of radius only and that the velocity at E_o is V_m. Then a seismic ray can be characterized by the constant ray parameter

$$p = \frac{r \sin i}{v} \qquad \text{(V-1)}$$

where v and i are the velocity and inclination of the ray from the radial direction at any radius r. Next, assume that over the dimensions of the array the variations of p with distance from the source, Δ, is approximately linear, i. e.,

$$\frac{dp}{d\Delta} = \text{constant} \qquad \text{(V-2)}$$

A more complicated variation of p with Δ could easily be incorporated if it were thought to be necessary.

Referring to Figure (12) let O' be a reference point in the array and O a point directly below it at the elevation E_o. Let A' be one of the array sites, and A be a point directly below it at the elevation E_o. Let the source be at an azimuth ω and denote the difference in the distance to the source between O' and A' by Δ_A. Consider the seismic wave with ray parameter p_o which arrives at the point O at time T_o. To a first approximation the same wave will arrive at the point A at the time

$$T_A = T_o + \Delta_A [p_o + \frac{1}{2} \frac{dp_o}{d\Delta} \Delta_A] \tag{V-3}$$

and the ray parameter at point A will be

$$p_A = p_o + \Delta_A \frac{dp_o}{d\Delta} \tag{V-4}$$

We now wish to calculate the time required for the wave to travel from A to A'. Above the elevation E_o the wave will be regarded as a plane wave. Referring again to Figure (12), let the elevation of A' be $E_{A'}$, and let the crust-mantle boundary below A' be at an elevation E_M and let it have a dip D in the azimuthal direction δ. Above this boundary the velocity is taken to be V_c and below it is assumed to be V_M. Then according to the results of Appendix A1 the wave will arrive at A' at the time

$$T_{A'} = T_A + \frac{E_{A'} - E_o}{V_M} \cos i + \frac{E_M - E_{A'}}{V_c} \left\{ \frac{V_c}{V_M} \cos v - [1 - (\frac{V_c}{V_M} \sin v)^2]^{\frac{1}{2}} \right\} \tag{V-5}$$

where i is the angle of incidence of the wave in the mantle given by

$$\sin i = \frac{p_A V_M}{R + E_o} \tag{V-6}$$

and R is the radius of the earth. The angle between the wave front and the crust-mantle boundary has been denoted by v and can be calculated from

$$\cos v = \cos i \cos D - \sin i \sin D \cos(\delta - \omega) \tag{V-7}$$

By combining equations (V-3) and (V-5) it is possible to calculate the arrival time of the wave at any point A' relative to its arrival time at the reference point O.

The horizontal phase velocity of the wave at the reference point O is given by

$$C_o = \frac{R + E_o}{p_o} \tag{V-8}$$

and thus

$$\frac{dC_o}{d\Delta} = - \frac{C_o}{p_o} \frac{dp_o}{d\Delta} \tag{V-9}$$

Thus, given the array geometry and its crustal structure, we can calculate the relative arrival times at the array sites for any wave having a phase velocity C_o and distance derivative $dC_o/d\Delta$. Conversely, given the relative arrival times, we can calculate the phase velocity of the incident wave.

The foregoing equations and the data of Tables 1 and 2 have been used to calculate tables of relative arrival times for all azimuths of interest at 0.2 degree intervals and all phase velocities between 8.0 km/sec and 26.0 km/sec at 0.2 km/sec intervals. The reference time for the relative times is taken as the average of the arrival times at the sites Z74 and Z63. Values of $dC_o/d\Delta$ can be determined by an iterative procedure since they have a second order effect. Initial values are assumed, a curve of C_o versus Δ constructed from the data, new values of $dC_o/d\Delta$ determined, and the process repeated. Two iterations are usually sufficient.

Relative arrival times of teleseismic P waves are measured on enlarged copies of the develicorder film and also on digital versions of the analog magnetic tape records. The measurements on the tape records, which are made with the aid of a computer, are superior to the film measurements since they avoid the possibility of optical distortion. The computer reads the magnetic tape records, digitizes the data at a rate of 10 samples per second, shifts the array channels in time by estimated amounts, and then displays the channels in parallel fashion on a direct writing visicorder. The time shifts are adjusted manually until it appears to the eye that the event of interest is aligned on all of the channels. Another program is available which automatically determines the necessary time shifts by maximizing the correlation function between the various channels. This program is sometimes used to assist the eyeball interpretation but it cannot be relied upon completely since it is sensitive to noise and sometimes gives obviously wrong results. As in the case of the theoretical calculations, the relative arrival times are determined with respect to the average arrival time on the two channels Z74 and Z63.

The measurement of relative arrival times has the advantage that it does not depend on an accurate recognition of the first motion and the times can be computed from any part of the waveform. In practice they are usually computed for the first prominent peak and the first definite zero crossing of the waveform and the results averaged. The arrival time of the first motion is measured for the channels of Z74 and Z63 and the results averaged to yield what is taken to be the absolute arrival time for the center of the extended array.

Having determined the relative arrived times, the calculated tables are searched for the velocity and azimuth which minimizes the root mean square error between the observed and calculated times. The error is determined by the equation.

$$\sigma = \left[\frac{1}{J}\sum_{j=1}^{J}(\Delta T^{j}_{obs} - \Delta T^{j}_{calc})^2\right]^{\frac{1}{2}} \qquad \text{(V-10)}$$

where J is the number of channels and ΔT^{j}_{obs} and ΔT^{j}_{calc} the observed and calculated relative arrival times, respectively, for the j-th channel. The absolute arrival time, phase velocity, azimuth, and root mean square error are all recorded. If the error is greater than 0.1 sec the measurements are rechecked.

G. Measurement of Relative Amplitudes

It is also possible to measure the relative amplitudes of a seismic wave at the various sites of an array. The use of an array to measure the rate at which amplitude is changing with distance is potentially a more sensitive method than the usual one of measuring absolute amplitude at a single station. The array method of relative amplitudes is essentially independent of the source and propagation factors such as magnitude, radiation pattern and attenuation along the path. The use of such data in conjunction with array measurements of phase velocity may reveal properties of the velocity structure of the mantle which were previously concealed by the averaging process which had to be used.

The personnel at TFSO daily calibrate each seismometer of the extended array with a 1 cps sine wave and calculate its

magnification. (Average magnification at TFSO is about 560K.) At Cal Tech the standard practice has been to measure the amplitudes of a particular event on enlargements of the develicorder film. The period and one half the peak to peak amplitude are measured for a prominent portion of the first two cycles of the event. This measurement can be reduced to an equivalent ground motion by taking account of the optical magnification involved in enlarging the film, the magnification of the seismometer system for that particular day, and the frequency response of the seismometer as given in Figure (9). The equivalent ground motion is calculated in this manner for each channel of the array and the results plotted as a function of the relative distance from the source. The resulting points are fitted with a straight line and its slope and intercept at zero time determined. The latter is taken as the absolute amplitude at the center of the array.

There are reasons to suspect that one of the major sources of error in the determination of relative amplitudes on the extended array is the measurement of period. Teleseismic waves normally have a dominant period in the 0.5 to 3.0 sec range. Examination of the seismometer response curves given in Figure (9) reveals that in this range a small error in the period measurement can cause a large error in the equivalent ground motion. This problem is intensified by the inherent difficulty of measuring the dominant period of a pulse in the presence of noise.

H. Application of Nonlinear Methods

As pointed out in Section 3, the choice of the optimum processing method for a particular array is determined primarily

by the characteristics of the noise. Dean (1965) and the Seismic Data Laboratory Report (1965) present the results of signal and noise analysis for the extended array at TFSO. The Texas Instruments Report (1965) contains a noise analysis more applicable to the 31 element circular array. Dean (1965) concludes that signal and noise correlations decrease with an increase in either the frequency or distance, that the noise appears to be random between two sites separated by more than 30 km, that the signals retain some correlation up to 800 km, and that signal correlation predominates over noise correlation for all distances greater than 3 km.

The preceding results concerning the noise properties indicate that the linear processing methods discussed in Section III, which depend upon well organized noise for their efficiency, would be severely limited if applied to the extended array. Because of this, most of our efforts have been directed towards developing, the nonlinear methods of Section IV into an effective processing scheme for the extended array. Another reason for going to nonlinear methods is pointed out by Birtill and Whiteway (1965). They showed that the wavenumber response appropriate for the correlation between the sums of the two legs of a cross array is considerably better than that obtained by summation alone. Such a calculation was made for the extended array and the results are contoured in Figure (13). A comparison of this figure with the summation results of Figure (10) shows that both the aperture width and the magnitude of the side lobes are smaller for the nonlinear correlation method.

These reasonings and the experimentation that followed have led to the adoption of a processing scheme for the extended array which has proved very satisfactory for the analysis of teleseismic P waves. Although the method is nonlinear in principle, an attempt

was made to retain some of the desirable properties of linear processing, such as a reasonably small amount of signal distortion.

Figures (14), (15) and (16) are the result of applying the complete array processing scheme to a teleseism from northern Chile. The earthquake occurred on May 2, 1965, was at a depth of 117 km and had a magnitude of 5.5. The epicenter was 66.9 degrees from TFSO at an azimuth of 137.0 degrees. Figure (14) is a reproduction of the original 12 channels of data. Traces 1 to 6 correspond to the NW-SE leg of the array and Traces 7 to 12 to the NE-SW leg. The data have been sampled at a rate of 10 samples per second.

Figure (15) is the output of the array processing program for the input data of Figure (14) after they have been given time shifts appropriate for a phase velocity of 17.2 km/sec. Traces 1 and 2 are just reproductions of two of the original data channels, channels Z70 and Z67 in this case. Trace 3 is the normalized sum of all 12 data channels. Trace 4 is the normalized sum of the 6 channels on the NW-SE leg of the array after a digital filter has been applied to each individual channel. Trace 5 is a similar result for the NE-SW leg of the array. The digital filters are arbitrary and may be different for each channel. In this case only two different 21 point filters were used and these were chosen so as to compensate for the different frequency response of the two different types of seismometers used on the extended array. Trace 6 is the average of Traces 4 and 5. Trace 7 is the vela time code. Trace 8 is the result of applying the nonlinear processing scheme described in Section IV to Traces 4 and 5. A 1.0 sec correlation window was used and an 0.5 sec filter window. The filter coefficients at each instant have been constructed according to equation (IV-4) with the exception that a small positive

constant has added to the denominator. This increases the numerical stability of the calculations and can be thought of as a small level of constant noise. Trace 9 is a reproduction of Trace 8 at a reduced scale of 1/4. Trace 10 is similar to Trace 8 except the filter coefficients are not normalized for the signal and noise power. That is, the procedure is identical to that used to obtain Trace 8 except the denominator of the filter coefficients as given in equation (IV-4) is set equal to 1.0. Trace 11 is an attempt to determine the polarity of the seismic pulses. It is the result of convolving a typical seismic pulse with Trace 8. The first arrival may be inserted as the typical pulse in order to pick out later arrivals having the same shape. For the most part, this trace has been of little value. Trace 12 is the zero-lag normalized cross correlation between Traces 5 and 6, which is the center point of the nonlinear filter and is given by equation (IV-4) with $\tau = 0$. This trace is not synchronous with the other 11 channels and leads them by 2.0 sec.

In Figure (16), the nonlinear filter output, Trace 8 of Figure (15), is shown for several different values of phase velocity. Several of the prominent phases are labeled on the trace where they appear to be best developed.

VI. VELOCITY MEASUREMENTS OF TELESEISMIC P WAVES

Jeffreys and Gutenberg both made comprehensive studies of the travel times of teleseismic body waves and constructed velocity models for the mantle on the basis of these studies. The data of both studies consisted primarily of first-arrival times of principal phases, although Gutenberg supplemented this with amplitude data. In studies such as these the velocity model is constructed by plotting the first-arrival times, fitting them with a curve, determining apparent phase velocities from the slope of the curve, and then numerically integrating the phase velocity data by the Wiechert-Herglotz method to determine the velocity as a function of depth.

Note that in the procedure mentioned above the measurement of the apparent velocity depends upon the determination of the slope of an empirical curve. Errors in origin times and epicenter locations contribute to the scatter of the data. In fitting such data the experimenter is faced with the problem of separating real variations from scatter due to errors, and the result is the smoothest possible curve which is consistent with the data.

Thus there is a natural bias against abrupt changes in the slope of the curve. Such a bias does not have a very important effect upon the travel time curve itself, but it may lead to the elimination of certain character of the apparent velocity curve.

Problems of this type can be avoided to a large degree by measuring the phase velocity with an array, because the phase velocity is measured in a more direct manner and the determination is not influenced by error in the origin time. This reasoning was the basis of the present project of using a large array to measure phase velocities of teleseismic P waves in the 30 to 100 degree range.

A. Collection of the Data

All teleseisms in the period April 15 to July 25, 1965, which wrote a clearly observable direct P wave at TFSO have been cataloged and their distance and azimuth from TFSO calculated by using the epicenter coordinates given by the U. S. Coast and Geodetic Survey.

Absolute and relative travel times as well as amplitudes were measured and phase velocities determined by the methods outlined in Section V for a total of 125 teleseisms. The results are listed in Table (3) and plotted in Figures (17), (20) and (22). All distances and times appearing in the table and figures have been corrected to a source depth of 33 km assuming a Gutenberg model of the earth. The times also contain an ellipticity correction which amounts to a maximum correction of 1.8 sec for this data. At least 6 and in the majority of the cases all 12 channels of the array were operating and readable for the events listed. Obvious after-shock sequences were avoided since they usually give very similar results, which leads to an unequal weighting of the data.

The root-mean-square errors of the phase velocity determinations are included in Table (3) as a measure of the goodness of fit. The times were read to the closest 0.1 sec and the generally small value of the root-mean-square error reflects the fact that it was possible to obtain reasonably good fits between the observed relative arrival times and the values predicted for a particular velocity; it also indicates that the crustal model used to predict the relative arrival times is reasonably appropriate. The data have been grouped according to azimuth and in the various figures each quadrant has been given a separate symbol. No obvious azimuthal dependence

appears in the data and this can be taken as additional evidence that an appropriate crustal model has been used in the reduction of the data. These comments about the crustal model should be interpreted with caution, however, because it is difficult to separate the effects of the crust from other effects along the propagation path. Furthermore, other crustal models could probably be designed which would fit the data equally well. These comments also should not be taken to imply that the mantle is laterally homogeneous; however, no mantle variations were required to remove an azimuthal dependence.

In the worst possible case two waves which differ in phase velocity by 0.2 km/sec would cross the array with a relative time difference of 0.1 sec, which is the accuracy of the time measurements. Thus it is believed that the average error of the phase velocity measurements is $\pm$ 0.2 km/sec. The scatter in the data appears to substantiate this estimate. Epicenters are from the refined determinations of the Coast and Geodetic Survey except for those of July which are based upon the preliminary determinations.

This report is based upon earthquakes with epicenters between 30 and 100 degrees from TFSO. Thus the deepest points of the observed waves lie between a depth of about 800 km and the earth's core. This corresponds to all of Bullen's region D and a portion of region C. Below a depth of 1000 km the velocity models of Gutenberg and Jeffreys are in fair agreement and both are relatively smooth. This latter fact is the basis of many arguments for chemical homogeneity in the lower mantle. A comprehensive summary of the present state of seismic knowledge concerning this region as well as the rest of the mantle has been provided by Anderson (1966).

B. Interpretation of Phase Velocity Data

The phase velocity data have been plotted in Figure (17) and the solid line labeled CTP4 is a smoothed fit to the data between 30 and 100 degrees. The fit is good at distances less than 85 degrees but the number of rather low phase velocities at larger distances is a surprising result. An attempt to correlate the velocities at this distance with azimuth failed. The triplication of the phase velocity curve as shown by CTP4 appears to be the best interpretation of the data. The dashed line labeled CTP3 in Figure (17) is a more conventional interpretation of the data which ignores the lower velocities at large distances.

In either case the velocity structure of the lower mantle is clearly more complicated than the standard structures of Jeffreys or Gutenberg. In addition to the complexities beyond 85 degrees, points of increased curvature in the phase velocity curve appear at distances of 36, 43, 51, 60, 68 and 76 degrees. It should be emphasized that the curve shown in Figure (17) is the smoothest one consistent with the data. The accumulation of more data and the examination of later arrivals may tend to increase these second-order discontinuities.

Given a phase velocity curve such as that of Figure (18) it is possible to calculate the velocity as a function of depth by the Wiechert-Herglotz method. This consists of evaluating the integral

$$\log\left(\frac{r}{R}\right) = -\int_0^{\Delta} \cosh^{-1}\left(\frac{C(\Delta)}{C(\Delta')}\right) d\Delta' \qquad \text{(IV-1)}$$

for each point on the phase velocity curve. The velocity corresponding to r is then given by

$$v = \frac{r}{R} C(\Delta) \qquad \text{(VI-2)}$$

The validity of the results obtained by this method depends upon the assumption that the quantity r/v is monotonically decreasing with depth which may not be true in a low velocity zone. There appears to be no published evidence for such a zone in the lower mantle and it seems very unlikely that the effects of an appreciable low velocity zone, such as that proposed for the upper mantle, could have gone unnoticed by the many investigators of teleseismic P waves. We shall proceed to assume that r/v is monotonically decreasing in the lower mantle. An exception may be the extreme bottom of the mantle where the effects of the core boundary complicate the data. Some investigators, such as Dahm (1934), have proposed a decrease in velocity with depth for this region.

Because our data does not extend to zero distance, it is necessary to assume a velocity model for the upper mantle. Then the earth is stripped by the method of ray tracing to an appropriate depth and the Wiechert-Herglotz method applied to the phase velocity curve which would be observed at this depth in order to determine the velocity at greater depths.

In order to determine the effects which the assumed upper mantle model has upon the velocity-depth relation calculated for the lower mantle, the procedure was repeated for five different upper mantle models. The earth was stripped to a depth of 771 km in each case. The results are plotted in Figure (18). The resulting structures and the upper mantle models are as follows:

CTP1 - Jeffreys upper mantle.

CTP2 - Gutenberg upper mantle.

CTP4 - Modified version of Z model of Niazi and Anderson (1965).

CTP5 - Similar to CTP4 with higher velocities, especially near the top of the mantle.

CTP6 - Similar to CTP4 with higher velocities throughout the upper mantle.

In order to be consistent with the phase velocity measurements which were computed assuming a velocity of 7.85 km/sec at the top of the mantle, all of the upper mantle models were constrained to have the same velocity at this point. This does not have an appreciable effect upon the results.

As noted previously, the model CTP3 is based on the dashed curve of Figure (17) which ignores the low values of observed phase velocities beyond 85 degrees. Except for the bottom 250 km of the mantle it is identical to CTP4. In a study based upon travel times alone, this would be the most probable interpretation.

From Figure (18) it is clear that the primary effect of the upper mantle models upon the lower mantle structure is a slight shift in the complete curve. An exception occurs near the junction of the assumed and calculated models at a depth of 771 km where the data suggests a rather pronounced second-order discontinuity. On the basis of the data presented here it is impossible to select one of the five upper mantle models as the "correct" one. The model CTP4 will be adopted for later comparisons and calculations because its upper mantle is based on the results which Niazi and Anderson (1965)

obtained from the analysis of data which was also recorded at TFSO. This model is also convenient for comparison because it is intermediate to those considered.

As mentioned previously the general shape of the velocity profile in the lower mantle does not depend critically on the velocity assumed for the upper mantle. At this stage the variation of velocity with depth is our main concern. For the sake of comparison the model CTP4 has been plotted in Figure (19) along with the models of Jeffreys and Gutenberg.

Note the pronounced discontinuity at a depth of about 840 km for the CTP4 model. Unfortunately, the close proximity of the discontinuity to the bottom of the assumed upper mantle model makes an exact interpretation of its depth and abruptness difficult. However, consideration of the fact that it exists for a wide range of upper mantle structures (Figure 18) leaves little doubt that it is real. One should also keep in mind that this may be only a part of a feature which begins at a shallower depth.

The Gutenberg model also has a discontinuity at a slightly greater depth. Anderson (1966) summarizes evidence for an upper mantle discontinuity starting between 600 and 700 km. It should also be noted that the 720 km level marks the lower bound for tectonic activity. Anderson (1966) also points out that the ratio of compressibility to rigidity reverses its trend at about 800 km and suggests that the boundary between Bullen's region C and region D can probably be placed between this depth and 1000 km. Thus the second order discontinuity which we have proposed for a depth of 840 km is consistent with observations if we interpret it as the termination of a region of relatively rapidly increasing velocity which begins between 600 and 700 km. The models CTP4, CTP5,

and CTP6 of Figure (18) have this type of structure. Future work of extending the phase velocity curve to shorter distances should clarify this feature. The study of later arrivals will be particularly important in the interpretation of future work on the upper mantle.

Another second-order discontinuity of the CTP4 model occurs at a depth of 1150 km which again is slightly shallower than a similar discontinuity in the Gutenberg model. Evidence for this discontinuity appears on the phase velocity curve between 45 and 50 degrees. Other less pronounced indications of second-order discontinuities occur at depths of about 1320, 1700 and 1950 km. The effects on the phase velocity curve appear at distances of 55, 65 and 71 degrees, respectively. Also note that below a depth of 1500 km the CTP4 model has significantly lower velocities than those of Gutenberg or Jeffreys.

Proceeding downward to the region near the core boundary, we observe that the CTP4 model differs considerably from those of Jeffreys or Gutenberg. The CTP4 model has a region of almost constant velocity of 13.50 km/sec between depths of 2670 and 2800 km and then rises abruptly to a value of 13.65 km/sec at a lower bound of 2881 km. The region adjacent to the core could be approximated by a high velocity layer between 50 and 100 km thick. Note that there is actually a slight decrease in the velocity near a depth of 2790 km, but as expected, the critical quantity r/v remains monotonically decreasing. If we were to assume the more conventional interpretation represented by the model CTP3 in Figures (17) and (18), then the velocity rises smoothly to a value of 13.71 km/sec at a depth of 2866 km. This is close to the 13.70 km/sec value found for the base of the mantle by Gutenberg. Further comments about the core boundary will be deferred to a discussion of PcP travel times which follows later.

C. Interpretation of Travel Time Data

In addition to relative travel times, absolute travel times to the center of the array were also measured. These are plotted as residuals from the Jeffreys-Bullen (JB) Tables in Figure (20). The data show a considerable scatter which is not unusual for times based upon earthquakes. However, it is obvious that the times are predominantly late compared to the JB Tables. This is characteristic of TFSO. For instance, the West Virginia earthquake of November 25, 1964, was at a distance of 24 degrees and had a JB residual of +3 sec (Seismic Data Laboratory, 1965). The recent Long Shot explosion was at a distance of 52 degrees from TFSO and had a JB residual of -2.5 sec (Seismic Data Laboratory, 1966). However, this was at least 1 sec later than the average of other stations for this event.

An important check on the velocity-depth structure which we have calculated from the phase velocity data is that it should be consistent with the observed travel times of P. Note that the phase velocity and travel times are determined independently in the present method, whereas this is not true of the conventional method of using travel times to derive a velocity structure.

Travel times were calculated for the model CTP4 and plotted in Figure (20). A 33 km thick crust with a velocity of 6.2 km/sec was assumed for the calculations. There appears to be a real discrepancy between the observed and calculated times. The calculated times are late at large distances and exhibit a strong dependence upon distance. It appears that the model CTP4 may have a region of too low velocity. Such a region could be in either the upper or lower mantle but since the upper mantle is an assumed structure we will consider it first.

The hypothesis that the upper mantle of the model CTP4 contains velocities that are too low can be checked by considering the models CTP5 and CTP6 which were designed with this partially in mind (Figure 18). Both have structures roughly parallel to that of CTP4 with CTP5 having higher velocities mainly near the top of the mantle while CTP6 has higher velocities throughout the upper mantle. Travel times were calculated for both of these models and parallel results were obtained. The travel time residual curve was shifted in the direction of more negative residuals without any appreciable change in its shape. Thus this hypothesis was discarded as a possible explanation of the discrepancy between the observed times and those calculated for the models.

Turning to the lower mantle as a possible cause of the discrepancy, we have considered the possibility that the hypothesized second-order discontinuities of the model CTP4 are larger than shown. Note that inserting a small discontinuity in the velocity structure will affect the observed phase velocities over only a small range of distances and leave the rest of the phase velocity curve unaffected. However, the affect upon travel times may be quite large since all velocities at a lower depth are altered. This points out the importance of measuring phase velocities and travel times independently and comparing the results.

In order to test this hypothesis one of the second-order discontinuities of the CTP4 model was slightly increased and travel times calculated for the resulting model. The discontinuity at a depth of 1320 km was increased because the affects of this depth first appear at a distance of 50 degrees and the JB residuals for the CTP4 model begin to increase at this distance. The discontinuity was increased such that all velocities at lower depths were increased by

0.06 km/sec. The result is shown in Figure (19) as CTP7 and the calculated JB residuals are plotted in Figure (20). The JB residuals of the CTP7 model are much more in agreement with the observed residuals than those of CTP4, and it is evident that even better agreement could be obtained by altering discontinuities which are hypothesized for other depths. However, this exercise has already served its purpose in that it has pointed out the major importance of accurately measuring any second-order discontinuities which may exist in the velocity structure.

At this stage the model CTP7 cannot be proposed as a final model for the lower mantle structure because it does not come directly from the data although it does not contradict the available data. However, it is interesting to note that the triplication which appears on the travel time curve at about 50 degrees (Figure 20) is very small and would be lost in the scatter of travel time measurements. The affect upon the phase velocity curve is more pronounced and consists of a step of about 0.2 km/sec with a slight triplication at a distance (50 degrees) which had previously been interpreted as a more gradual rise in the curve (Figure 17). The model CTP7 does not contradict the data and this serves to emphasize the fact that more data must be gathered in order to determine whether such features exist at this distance and also other distances. Future work will be directed toward this end with special attention being paid to amplitude, secondary arrivals, and velocity filtering.

Note that we have not completely resolved the discrepancy between the observed travel times and those calculated for our velocity structure. We have only shown that additional or increased discontinuities in the velocity structure is a possible solution. Additional analysis will be required to resolve this problem.

The phase PcP provides another check on the calculated velocity structure. In an analysis of P and PcP signals from the BILBY explosion, Buchbinder (1965) finds that the JB residuals average -1.34 sec for P and -1.80 sec for PcP. He suggests this discrepancy can be explained by increasing the velocity in the Jeffreys model of the mantle or by decreasing the depth to the core by not more than 10 km.

Note that the model CTP4 is based on data which extends only to a distance of 96 degrees. Other earthquakes with distances up to 98 degrees are included in this study but their phase velocities do not fall on the upper branch of the phase velocity curve. Thus we have had to assume that the shadow zone starts at 96 degrees. It is interesting to note that if this is truly the case and if the phase velocity curve of Figure (17) is valid, then sharp arrivals corresponding to the lower branch of the phase velocity curve will be observed out to a distance of 98 or 99 degrees and this would mask the fact that the true shadow zone begins at 96 degrees.

Assuming the phase velocity curve of Figure (17) is correct then we can calculate that the lower bound on the depth of the core is 2881 km as compared to the standard value of 2898 km. Choosing to compare our data with that of Buchbinder at a distance of 40 degrees, we calculate JB residuals of +0.4 sec for P and +0.6 sec for PcP. This is not consistent with Buchbinder's results since he found a PcP residual which was 0.46 sec less than the P residual. The CTP4 model could be modified to conform to Buchbinder's results by decreasing the depth to the core or by increasing the velocity in the mantle. The former is not possible since the 2881 km value is already a lower bound. Thus these results indicate that the model CTP4 has too low velocities which is the same conclusion that the consideration of P travel times gave.

Let us now consider the model CTP7. This also has a lower bound of 2881 km and has residuals of +0.4 for P and -0.7 for PcP at 40 degrees. To make these results consistent with those of Buchbinder we must decrease the mantle velocity or, assuming that the velocity structure is correct, we must set the core depth to a value of 2887 km. The agreement between this value and the value of 2888 km which would explain the discrepancy which Buchbinder observed is most probably fortuitous because of the uncertainties which still remain in the CTP7 model. However, these results do indicate that if further investigations prove the CTP7 model or one similar to it to be valid, then the model can be easily adjusted to satisfy the PcP data of Buchbinder by setting the core depth about 6 km below the lower bound of 2881 km we had estimated on the basis of available data.

Referring again to Figure (20) let us consider the travel times beyond 85 degrees where the triplication of the travel time curve is hypothesized. The scatter in the observed data makes a critical comparison with the calculated curve extremely difficult. However, it may be possible to compare the calculated curve with the observed seismograms. With this in mind the seismograms of the four earthquakes which are beyond 90 degrees and lie on the lower branch of the phase velocity curve CTP4 of Figure (18) have been reproduced in Figure (21). The channels have been aligned in accordance with the measured phase velocities. The P waveforms are complex in all four cases and are typical when compared with those observed at shorter distances. The first Solomon event and the Greek event are similar in that a small precursor appears to precede the larger arrival by less than a second. Note that the phase velocity measured for these two earthquakes refers to the larger arrival since the precursor was too indefinite to measure

accurately. The P waveform of the second Solomon event is suggestive of the interference pattern expected for two arrivals slightly separated in time. The New Britain event has a waveform which is vague and long period and completely different from all the other events used in this study; it is similar to observations in the shadow of the core. The results of Figure (21) can be summarized by saying that the pictured waveforms are not inconsistent with a triplication of the travel time curve but at the same time they do not provide conclusive support of such a hypothesis.

The nonlinear processing scheme outlined in Section IV was applied to these earthquakes in the hope of separating different phase velocities but the close proximity of the pulses in both time and velocity make the results inconclusive. Another line of evidence which was not checked, and should be if investigation along these lines is to continue, is the collection of seismograms for these same earthquakes at different distances so as to verify that the complexities depicted in Figure (23) are not really source effects.

D. Interpretation of Amplitude Data

Relative amplitudes were also measured according to the method outlined in Section V. Since the primary objective was the rate of change of amplitude with distance it was possible to measure the amplitudes of that portion of the P wave which was recorded the best on all of the channels. This was not always the maximum motion but was always taken from the first two cycles of the signal. The amplitudes were reduced to ground motion in millimicrons by correcting for the magnification and frequency response of the instrument. The amplitudes A could then be regarded as a function of relative distance and fitted with a least-squares straight line to

yield an estimate of the $dA/d\Delta$. This method was only applied to earthquakes which wrote clear on-scale records on the develicorder film and which occurred on days when adequate calibrations were available. The results are listed in Table 3 and are plotted in Figure (22).

In order to check the observed amplitudes against those predicted by the lower mantle structure which was derived earlier in this section, amplitudes have been calculated for the structure CTP4. If only the effect of geometrical spreading is considered, the following relation holds for the amplitude A (Gutenberg, 1944)

$$A \sim \left[\frac{d(\cos(i_s))/d\Delta}{\sin(\Delta)\cos(i_o)} \right]^{1/2} \qquad \text{(VI-3)}$$

where i_s and i_o are the angles of incidence at the source and receiver, respectively. Values of $d(\cos(i_s))/d\Delta$ were calculated by differencing calculated travel times and the resulting values of A are plotted for a surface source in Figure (23). Note that equation (VI-3) implies the following relation

$$A \sim f\left(\frac{d^2T}{d\Delta^2}\right) \sim f\left(\frac{dC}{d\Delta}\right) \qquad \text{(VI-4)}$$

Thus it is interesting to compare the amplitude of Figure (23) with the phase velocity curve of Figure (17). The peaks in the amplitude curve correspond to the regions of maximum slope in the phase velocity curve which is what equation (VI-4) predicts. If Figure (23) is compared with the similar plots given by Gutenberg (1958) one finds fair agreement for the peaks near 43 and 60 degrees.

In Figure (23) values of A have been plotted for the various branches which comprise the triplication of the travel time curve for CTP4. However, these values should be interpreted with caution because they are very sensitive to the manner in which the curve was fit to the phase velocity data and a slight change in the fit might alter the predicted amplitudes considerably.

Let us now compare the values of A calculated for the model CTP4 with the observed values of $dA/d\Delta$. If such a comparison is to be rigorous, the observed values of $dA/d\Delta$ must be normalized for the magnitude and radiation pattern of the source and the calculated values of A must include the effect of attenuation. However, such rigor is not completely necessary because a considerable amount of information is contained in only the sign of $dA/d\Delta$. In particular, knowledge of the sign of $dA/d\Delta$ would be a great aid to the interpretation of phase velocity data in as much as it tells one whether the phase velocity curve has positive of negative curvature; furthermore, the zero crossings of $dA/d\Delta$ denote the points of maximum or minimum slope on the phase velocity curve. On the basis of such reasoning the sign of $dA/d\Delta$ for the model CTP4 has been taken from the curve of Figure (23) and plotted in Figure (22). There appears to be a correlation between the sign of the observed and calculated values of $dA/d\Delta$ and this is encouraging, especially in view of the rather complicated variation of this quantity with distance. Note that if a more detailed analysis of the $dA/d\Delta$ data were to be made, one should plot $d(\log A)/d\Delta$ instead of $dA/d\Delta$. This would normalize for the effects of the signal size.

A comment on the scatter of the data in Figure (22) seems appropriate. The periods of the measured P arrivals fall between 0.7 and 1.4 sec and waves of this frequency see many of the minor

features of the crust which may vary from one station to the next. As pointed out in Section V, the response characteristics of the instruments are changing rapidly in this frequency range which means that the calculated amplitudes depend critically upon a precise measurement of the period of the signal; such a measurement is always difficult when dealing with pulses and additionally so when noise is present. This disadvantage could be partially avoided by pre-filtering the seismograms to remove the instrument response before measuring the amplitude. The inclusion of station amplitude factors for each site of the array would undoubtedly improve the data. The accumulation of more data will possibly permit the determination of these station factors.

VII. SUMMARY

The purpose of this thesis was to efficiently use a large seismic array to obtain information about the variation of compressional velocity with depth in the earth's lower mantle. This necessitated a review of some of the basic concepts involved in the processing of data from a seismic array.

Several linear methods of processing were reviewed and it was pointed out that these methods depend upon the organization of the noise for their efficiency. In the case of uncorrelated noise these methods all reduce to a simple time shift and summation.

A nonlinear method of processing a large array which has proved quite effective for the removal of uncorrelated noise was described. It was also shown that by proper choice of the correlation window length and the filter window length, coherent signals can be separated from the noise without extreme amounts of distortion.

The application of array processing techniques to one particular array, TFSO in central Arizona, was considered in detail. Methods for measuring phase velocities, times, and relative amplitudes were described. Examples of the application of nonlinear processing were also given.

Phase velocities were measured for teleseismic P waves at epicentral distances between 30 and 100 degrees in an attempt to determine the velocity as a function of depth in the lower mantle. The phase velocities were fit with a single smooth curve except at distances beyond 85 degrees where unexpectedly low velocities were interpreted in terms of a triplication of the phase velocity curve.

A variety of upper mantle models were assumed and the phase velocity curve inverted by the Wiechert-Herzlotz method to obtain a velocity depth structure for the lower mantle. The effect of the various upper mantle models is to shift the lower mantle structure to higher or lower velocities without appreciably changing the shape of the structure.

The velocity structure which was calculated for the lower mantle contains a pronounced second-order discontinuity at a depth of 840 km, another at 1150 km, and less pronounced indications of second-order discontinuities at depths of 1320, 1700 and 1950 km. The interpretation of the phase velocity data in terms of a triplication results in a structure near the core boundary which differs considerably from those of Jeffreys or Gutenberg. A 130 km thick zone of approximately constant velocity lies above a 50 to 100 km thick zone of higher velocity.

The importance of comparing independent observations of travel times and phase velocities as a consistency check is emphasized. When this check is applied to the calculated velocity model for the lower mantle it indicates that the lower mantle has too low velocities. One possible solution to this problem is to increase one or more of the second-order discontinuities in the lower mantle. An alternate velocity structure is constructed in this manner which gives closer agreement with the observed times for P, and this model is also consistent with times for PcP if the depth to the core is about 2887 km. In any case the data indicates a lower bound of about 2880 km for the core depth if the interpretation of the phase velocity curve is assumed to be right.

At this stage, the calculated velocity structures cannot be seriously proposed as models for the lower mantle because of the uncertainties caused by the assumption of an upper mantle structure.

The accumulation of more data and the extension of phase velocity measurements to shorter distances should improve this situation. Nevertheless, on the basis of the present data, it appears that the lower mantle is more complicated than the models of Jeffreys or Gutenberg with good evidence for second-order discontinuities below a depth of 1000 km.

To the author's knowledge, no one has previously tried to measure and interpret values of $dA/d\Delta$ with an array. This was attempted in order to ascertain if $dA/d\Delta$ could be a useful measurement. The results were not conclusive but definitely promising. The fact that $dA/d\Delta$ provides useful data which is relatively independent of assumptions about the magnitude and radiation pattern of the source is probably its main asset. Another advantage is that knowledge of the sign alone of $dA/d\Delta$ is often of considerable value in the interpretation of phase velocities. Thus, in view of these results and also the invaluable role which amplitude data can play in the interpretation of discontinuities in the velocity structure, it is concluded that this method is well worth future use and development.

The general conclusion of this report is that a seismic array is a powerful tool for extracting information from seismic waves. Although the proposed models for the lower mantle velocity structure are not final, they are probably based on more information than previous lower mantle models. The importance of using all the available data - phase velocity, travel times, amplitudes, and secondary arrivals - cannot be overemphasized.

APPENDIX A1

TRAVEL TIME ACROSS A DIPPING INTERFACE

In this appendix we will derive an expression for the travel time of a plane wave crossing an arbitrarily oriented plane boundary between media of different velocities.

Shown in Figure (24) is a plane wave surface W a distance d from the origin with normal $\vec{w}$ and direction cosines a, b and c. Its equation is

$$W: \quad ax' + by' + cz' - d = 0 \tag{A1-1}$$

The perpendicular distance from W to any point P(x, y, z) is

$$r' = - (ax + by + cz - d) \tag{A1-2}$$

and the distance of P from the origin is

$$r = \sqrt{x^2 + y^2 + z^2} \tag{A1-3}$$

Now require that P lie on the surface S which is at a depth h below the origin and has the normal $\vec{s}$.

$$S: \quad lx' + my' + nz' + nh = 0 \tag{A1-4}$$

Note that the angle between $\vec{w}$ and $\vec{s}$ is given by

$$\cos \eta = al + bm + cn \tag{A1-5}$$

Let S separate media of velocities v above and V below. Then the travel time from the wave surface W to the origin is

$$T = \frac{r'}{V} + \frac{r}{v}$$

$$= - \frac{(ax + by + cz - d)}{V} + \frac{\sqrt{x^2 + y^2 + z^2}}{v} \qquad \text{(A1-6)}$$

Requiring that T be a minimum time path subject to the condition that P lie on S is equivalent to minimizing

$$U = T + \lambda (lx + my + nz + nh) \qquad \text{(A1-7)}$$

with respect to x, y, z and λ. Thus we have

$$\begin{aligned} - \frac{a}{V} + \frac{x}{vr} + \lambda l &= 0 \\ - \frac{b}{V} + \frac{y}{vr} + \lambda m &= 0 \\ - \frac{c}{V} + \frac{z}{vr} + \lambda n &= 0 \\ lx + my + nz + nh &= 0 \end{aligned} \qquad \text{(A1-8)}$$

These equations can be combined to yield

$$(al + bm + cn) \frac{v}{V} - \lambda v + \frac{nh}{r} = 0 \qquad \text{(A1-9)}$$

and elimination of λ yields

$$\left(\frac{nh}{r}\right)^2 = 1 - \left(\frac{v}{V}\right)^2 (1 - \cos^2\eta) \qquad \text{(A1-10)}$$

which is equivalent to Snell's law. The combination of equations (A1-6), (A1-8), (A1-9) and (A1-10) yields the desired relation

$$T = \frac{d}{V} + \frac{nh}{v}\left[\frac{v}{V}\cos\eta - \left[1 - \left(\frac{v}{V}\sin\eta\right)^2\right]^{1/2}\right] \qquad \text{(A1-11)}$$

REFERENCES

Anderson, Don L., Chapter 3, The earth's mantle, T. F. Gaskell, (ed), Academic Press, Inc., London, 1966 (in press).

Backus, M. M., J. Burg, D. Baldwin, and E. Bryan, Wide-band extraction of mantle P waves from ambient noise, Geophysics, 29, 672-692, 1964.

Birtill, J. W., and F. E. Whiteway, The application of phased arrays to the analysis of seismic body waves, Phil. Trans. Royal Society of London, Series A, 250, 421-493, 1965.

Buchbinder, G. R., PcP from the nuclear explosion Bilby September 13, 1965, Bull. Seismol. Soc. Am., 55, 441-461, 1965.

Burg, John P., Three-dimensional filtering with an array of seismometers, Geophysics, 29, 693-713, 1964.

Capon, J. and R. J. Greenfield, Asymptotically optimum multidimensional filtering for sampled-data processing of seismic arrays, Technical Note 1965-57, Lincoln Laboratory, M. I. T., 1965.

Cramer, Harald, Mathematical Methods of Statistics, Princeton University Press, 575 p., 1946.

Dahm, C. G., A study of dilatational wave velocity in the earth as a function of depth, based on a comparison of P, P' and PcP phases. Dissertation, St. Louis University, 1934.

Dean, W. C., P-wave correlations and array alignments, in Data Processing Techniques for the Detection and Interpretation of Teleseismic Signals, Seismic Data Laboratory, Proceedings of the IEEE, 53, 1860-1884, 1965.

Gutenberg, B., Energy ratio of reflected and refracted seismic waves, Bull. Seismol. Soc. Am., 34, 85-102, 1944.

Gutenberg, B., Velocity of seismic waves in the earth's mantle, Trans. Am. Geophys. Union, 39, 486-489, 1958.

Kelly, E. J., M. J. Levin, Signal parameter estimation for seismometer arrays, Technical Report 339, Lincoln Laboratory, M. I. T., 1964.

Kelly, E. J., A comparison of seismic array processing schemes, Technical Note 1965-21, Lincoln Laboratory, M. I. T., 1965.

Lincoln Laboratory, M. I. T., Seismic Discrimination, Semiannual Technical Summary Report, 31 Dec., 1964.

Lincoln Laboratory, M. I. T., Seismic Discrimination, Semiannual Technical Summary Report, 17 July 1964.

Lincoln Laboratory, M. I. T., Seismic Discrimination, Semiannual Technical Summary Report, 30 June 1965.

Niazi, Mansour, Corrections to apparent azimuths and travel-time gradients for a dipping Mohorovicic discontinuity, Bull. Seismol. Soc. Am., 56, 491-509, 1966.

Niazi, Mansour, and Don L. Anderson, Upper mantle structure of western North America from apparent velocities of P waves, J. Geophys. Res., 70, 4633-4640, 1965.

Press, Frank, and Shawn Biehler, Inferences on crustal velocities and densities from P waves delays and gravity anomalies, J. Geophys. Res., 69, 2979-2995, 1964.

Robinson, E. A., Chap. 4, Scientific Report No. 8 of Contract AF 19(604)-7378, M. I. T., 1964.

Sax, R. L., and C. H. Mims, Rectilinear motion detection (Remode), Seismic Data Laboratory Report No. 118, Teledyne, Inc., 22 March 1965.

Seismic Data Laboratory, Teledyne, Inc., West Virginia earthquake, Long Range Seismic Measurements, Report No. 117, 1 March 1965.

Seismic Data Laboratory, Teledyne, Inc., Semi-Annual Technical Summary Report, 15 April 1965.

Seismic Data Laboratory, Teledyne, Inc., Long Shot, Long Range Seismic Measurements, Report No. 133, 5 January 1966.

Shimshoni, Michael, and Stewart W. Smith, Seismic signal enhancement with three-component detectors, Geophysics 29, 664-671, 1964.

Talwani, M., G. H. Sutton, and J. L. Worzel, A crustal section across the Puerto Rico trench, J. Geophys. Res., 64, 1545-1555, 1959.

Texas Instruments, Inc., Seismometer array and data processing system, Final Report, Phase 1, 1961.

Texas Instruments, Inc., Noise analysis for Tonto Forest Seismological Observatory, 1965.

Warren, David H., John C. Roller, and Wayne H. Jackson, A seismic refraction survey in the vicinity of the Tonto Forest Seismological Observatory, Arizona, (abstract), Trans. Am. Geophys. Union, 46, 155, 1965.

LIST OF TABLES

TABLE 1

Site Locations for Extended Array at TFSO

Code	Name	Lat. deg.	Long. deg.	Elevation km.	Distance from center* km.	Azimuth from center*
SGAZ	Seligman	35.64	113.26	1.68	236.05	310.10
JRAZ	Jerome	34.82	111.99	1.31	89.32	312.24
LGAZ	Long Valley	34.41	111.54	1.77	28.93	297.81
Z70	TFSO	34.31	111.30	1.47	4.25	306.94
Z67	TFSO	34.25	111.21	1.51	6.37	126.52
GEAZ	Globe	33.77	110.53	1.48	88.74	129.48
NLAZ	Nazlini	35.81	109.63	1.92	225.42	41.09
WOAZ	Winslow	34.88	110.62	1.58	88.75	41.77
HRAZ	Heber	34.67	110.77	1.87	62.72	47.13
Z74	TFSO	34.32	111.23	1.74	5.32	36.92
Z63	TFSO	34.25	111.30	1.55	5.28	216.93
SNAZ	Sunflower	33.86	111.69	0.88	61.16	220.05

* The center of the array is taken as site Z21 at TFSO with coordinates of 34.29 N. lattitude and 111.27 W. longitude.

TABLE 2

Crustal Structure for Extended Array Sites at TFSO

Code	Crustal Velocity km/sec	Depth to Moho, km	Dip to Moho, deg	Azimuth of Dip, deg
SGAZ	6.2	36.0	6.0	41.0
JRAZ	6.2	38.0	6.0	41.0
LGAZ	6.2	35.0	5.0	41.0
Z70	6.2	34.0	5.0	41.0
Z67	6.2	34.0	5.0	41.0
GEAZ	6.2	36.0	6.0	41.0
NLAZ	6.8	40.0	0.0	
WOAZ	6.4	40.0	0.0	
HRAZ	6.3	40.0	0.0	
Z74	6.2	34.5	5.0	41.0
Z63	6.2	33.5	5.0	41.0
SNAZ	6.2	32.0	5.0	41.0

TABLE 3

Earthquake Data and Measurements

Date 1965	Location	O. h.	T. m.	Δ deg.	Azimuth deg.	h km	M	C km/sec	rms error sec	T m.	T s.	dA/dΔ mμ/deg.
April 18	Fiji	14	08	86.4	234.1	33	5.2	22.8	0.08	12	40.5	-1.4
29	Kurile	06	09	69.6	318.4	451	5.1	18.2	0.08	11	04.9	-
29	Tonga	07	53	79.4	240.7	33	4.5	20.0	0.08	12	05.2	-0.1
29	Fiji	09	44	88.2	240.2	540	5.2	23.6	0.07	12	49.7	-0.1
29	Mariana	11	19	92.3	289.9	134	5.2	24.2	0.08	13	09.4	-4.8
May 1	Alaska	01	58	34.3	330.0	13	4.6	12.7	0.11	06	46.7	-
1	Mariana	13	02	95.2	288.6	5	5.1	24.8	0.12	13	22.8	-13.8
1	Alaska	21	27	34.4	330.0	33	5.3	12.8	0.12	06	47.9	-10.9
2	N. Chile	05	47	67.3	137.0	117	5.5	17.2	0.19	10	55.9	1.0
2	Fiji	10	52	86.4	240.8	581	4.9	22.9	0.09	12	41.6	-1.2
3	El Salvador	10	01	28.7	130.8	23	5.1	12.5	0.15	05	57.9	0.6
3	Chile	16	09	71.7	138.5	114	5.6	18.0	0.10	11	20.6	-
4	Peru	12	10	62.4	138.0	78	4.5	16.3	0.12	10	22.3	0.6
5	N. Chile	03	00	67.7	137.4	96	4.6	17.1	0.13	10	57.3	1.1
5	Peru	09	13	58.9	94	4.7		15.6	0.18	09	58.6	1.8
6	Chile	02	25	71.9	139.4	90	5.1	18.1	0.09	11	22.9	6.0

TABLE 3 (cont.)

Date 1965	Location	O. h.	T. m.	Δ deg.	Azimuth deg.	h km	M	C km/sec	rms error sec	T m.	T s.	dA/dΔ mμ/deg.
May 8	N. Chile	11	32	72.8	143.1	35	5.4	18.3	0.10	11	28.1	4.3
9	Panama	14	11	38.5	129.6	56	5.1	13.2	0.16	07	21.9	1.2
9	Peru	19	58	49.3	132.3	108	4.8	14.3	0.10	09	11.1	1.4
11	Alaska	17	37	36.6	329.9	58	5.5	13.1	0.09	07	06.5	1.2
13	Bolivia	02	23	73.0	132.1	589	5.1	18.2	0.10	11	29.0	-
13	Columbia	04	13	44.3	124.3	126	5.3	14.0	0.11	08	10.3	-
13	Kurile	16	37	71.1	313.1	68	4.9	18.1	0.10	11	17.7	-1.5
13	Japan	19	23	87.6	308.2	324	4.8	22.8	0.10	12	47.3	-
15	Tonga	23	33	79.3	241.4	253	4.8	20.2	0.10	12	05.5	-1.3
16	Japan	05	40	81.6	311.1	76	4.3	20.8	0.14	12	18.1	-
16	Panama	15	51	39.4	130.8	33	4.8	13.3	0.14	07	29.3	1.0
19	Solomon	03	00	94.9	262.3	50	5.6	23.5	0.05	13	21.5	-
19	Fiji	04	21	83.9	237.2	81	5.5	21.6	0.10	12	28.8	1.2
19	Fiji	04	38	83.9	237.7	98	5.0	21.8	0.08	12	28.9	3.0
19	Columbia	10	58	44.1	124.1	98	4.8	14.0	0.10	08	08.4	-2.8
19	N. Britain	13	59	98.1	269.6	70	5.6	23.8	0.15	13	36.2	-8.8
19	Rat	22	07	54.2	312.5	35	5.3	15.0	0.06	09	25.6	-

TABLE 3 (cont.)

Date 1965	Location	O. h.	T m.	Δ deg.	Azimuth deg.	h km	M	C km/sec	rms error sec	T m.	T s.	dA/dΔ mμ/deg.
May 19	Fiji	23	32	86.3	240.1	552	5.4	22.9	0.09	12	42.0	-
20	N. Hebrides	00	40	91.1	253.1	16	5.6	24.5	0.14	13	02.4	-
20	Near	02	13	55.3	312.3	41	5.4	15.1	0.09	09	33.2	1.7
22	Andreanoff	10	24	50.5	311.9	89	4.6	14.5	0.10	08	57.9	0.6
22	Fiji	10	31	86.7	240.0	578	5.8	23.0	0.08	12	43.7	-
24	Japan	13	48	81.3	310.2	29	5.0	21.0	0.13	12	14.4	-2.8
26	Guatamala	04	58	27.8	132.6	39	5.2	12.3	0.21	05	49.1	-0.3
27	Argentina	12	18	73.1	137.0	190	4.5	18.1	0.10	11	29.1	-0.1
27	Unimak	12	56	42.0	314.6	33	5.0	13.6	0.14	07	51.6	-
28	Tonga	08	34	76.8	241.0	31	5.1	19.3	0.09	11	50.8	0.8
28	Near	18	14	54.8	312.6	67	5.0	15.1	0.10	09	29.9	1.1
31	Japan	08	38	84.3	309.4	124	5.5	22.2	0.09	12	31.0	-
31	Tonga	09	36	82.8	239.0	259	4.4	21.1	0.10	12	23.9	-
31	Japan	11	23	85.1	304.8	40	4.8	22.0	0.11	12	34.9	-
31	Nicaragua	20	46	32.6	129.0	28	4.7	12.8	0.14	06	32.2	-
June 2	Chile	02	05	80.6	150.9	18	5.1	20.4	0.09	12	11.8	-0.3
2	Samoa	03	18	76.2	241.1	33	4.9	19.3	0.13	11	47.9	-
2	Fiji	05	12	88.9	239.0	538	5.6	23.6	0.10	12	54.2	-6.8

TABLE 3 (cont.)

Date 1965	Location	O. h.	T m.	Δ deg.	Azimuth deg.	h km	M	C km/sec	rms error sec	T m.	T s.	dA/dΔ mμ/deg.
June 2	Fiji	09	19	85.7	242.6	631	5.4	22.7	0.07	12	37.9	-
2	Easter	13	57	39.0	171.5	33	5.0	13.4	0.14	07	25.6	-4.0
2	Easter	14	06	38.7	171.3	33	4.7	13.4	0.13	07	23.9	-
2	Fiji	14	45	85.6	242.8	636	5.3	22.7	0.08	12	38.1	-
2	Fiji	14	58	85.7	242.8	636	5.4	22.7	0.15	12	38.3	-13.3
2	N. Atlantic	23	40	60.4	90.4	33	5.8	15.8	0.16	10	07.8	-
4	Chile	08	05	84.6	155.3	33	5.4	21.9	0.10	12	32.4	-5.0
4	Mariana	13	31	89.9	291.6	62	4.9	23.0	0.13	12	57.7	-
4	Rat	15	02	52.3	311.4	35	5.3	14.8	0.18	09	11.8	-
4	Kermadec	15	26	90.9	233.4	222	5.3	24.2	0.12	13	02.8	-
5	Tonga	11	13	79.3	241.6	295	5.0	20.1	0.29	12	05.1	-1.3
6	Argentina	06	10	72.2	136.9	122	4.7	18.1	0.07	11	24.4	-1.8
11	Easter	01	34	68.8	176.5	31	5.1	17.7	0.04	11	02.8	-
11	Near	02	37	54.8	313.0	35	5.5	14.9	0.10	09	29.8	-
11	Tonga	03	20	78.8	240.2	95	4.5	19.9	0.08	12	03.3	-
11	Kurile	03	33	73.1	312.7	50	6.0	18.4	0.07	11	28.7	-
12	Kurile	05	40	73.0	312.0	24	5.8	18.5	0.08	11	29.8	-1.1
12	Japan	06	19	86.5	318.0	503	4.6	22.7	0.10	12	41.7	-2.2
12	Guatamala	16	35	27.5	133.2	33	4.5	12.3	0.22	05	45.9	1.8

TABLE 3 (cont.)

Date 1965		Location	O. h.	T m.	Δ deg.	Azimuth deg.	h km	M	C km/sec	rms error sec	T m.	T s.	dA/dΔ mμ/deg.
June	12	Chile	18	50	67.9	137.3	102	5.8	17.2	0.12	10	57.6	-
	13	Kurile	02	20	72.9	312.2	20	5.5	18.5	0.09	11	28.5	-0.2
	13	Japan	07	06	77.9	312.4	34	6.0	19.7	0.10	11	57.0	-2.5
	13	Kermadec	18	47	91.3	230.6	33	5.0	24.5	0.12	13	04.6	-1.5
	14	Atlantic	16	47	71.6	92.5	33	5.2	18.1	0.16	11	20.5	0.4
	15	Rat	04	46	52.6	310.3	29	5.5	15.0	0.06	09	13.0	0.2
	17	E. Kazakh	03	44	95.6	354.0	0	5.4	24.8	0.07	13	25.2	-
	17	Unimak	14	23	40.9	314.8	33	4.5	13.4	0.23	07	42.2	-
	18	Peru	22	45	58.0	134.7	111	5.5	15.6	0.11	09	52.9	-
	18	Japan	22	58	83.7	307.8	60	4.9	21.7	0.07	12	27.1	-
	19	Near	06	38	55.9	314.0	38	5.5	15.2	0.09	09	38.5	0.0
	19	N. Atlantic	11	09	55.1	42.4	33	4.5	14.7	0.32	09	33.1	-
	19	Kamchatka	12	50	62.3	318.0	61	5.1	16.6	0.09	10	21.7	-0.6
	20	Samoa	00	50	79.0	242.6	297	4.9	20.2	0.09	12	03.8	0.1
	20	Kurile	01	57	72.9	312.5	41	5.5	18.5	0.09	11	28.0	-0.1
	20	Kamchatka	21	51	63.8	316.7	45	4.7	16.9	0.06	10	32.6	-
	21	Columbia	09	27	45.5	118.9	169	4.1	14.0	0.09	08	19.7	-
	22	N. Chile	14	19	66.3	135.9	122	5.0	16.8	0.10	10	48.0	-
	23	Nicaragua	07	37	31.2	131.2	24	4.5	12.6	0.23	06	19.7	6.2

TABLE 3 (cont.)

Date		Location	O. h.	T m.	Δ deg.	Azimuth deg.	h km	M	C km/sec	rms error sec	T m.	T s.	dA/dΔ mμ/deg.
1965													
June	23	Kurile	08	49	63.1	314.9	35	4.7	16.6	0.09	10	27.5	-
	23	Kermadec	10	59	91.8	231.3	23	5.3	24.6	0.14	13	07.1	-
	23	Kodiak	11	09	35.9	321.1	33	5.7	13.0	0.18	07	00.1	-2.4
	23	Kodiak	12	23	35.8	321.2	33	4.7	12.9	0.18	06	59.6	-
	24	N. Chile	03	29	65.7	136.1	72	5.0	17.0	0.20	10	43.7	2.8
	24	Japan	04	48	88.0	311.3	356	5.3	23.2	0.10	12	49.3	-
	24	Fiji	14	08	84.9	237.1	102	5.5	22.8	0.24	12	34.3	-
	29	Kurile	02	04	72.8	312.6	37	5.5	18.5	0.08	11	27.8	-1.9
	29	Kurile	16	01	71.5	312.7	48	4.7	18.2	0.11	11	20.7	-0.8
	30	Rat	08	33	53.4	312.5	41	5.7	14.9	0.15	09	19.0	-
	30	S. Bolivia	11	12	70.6	135.2	170	5.1	17.8	0.07	11	14.5	-
	30	Kamchatka	12	36	62.4	317.8	63	5.1	16.6	0.06	10	22.2	-
July	1	Chile	04	54	70.9	137.9	91	5.1	17.7	0.11	11	16.8	-
	1	Mariana	07	16	89.9	291.8	86	5.0	22.8	0.14	12	58.2	-0.5
	1	Kurile	17	41	64.7	314.4	66	5.0	16.8	0.09	10	38.0	-0.5
	3	N. Atlantic	02	22	57.4	45.2	36	5.3	15.2	0.28	09	48.4	-
	3	Japan	15	24	84.6	308.9	125	4.5	21.9	0.07	12	32.6	-
	5	N. Atlantic	08	31	56.1	45.4	33	5.7	15.2	0.29	09	32.8	-
	5	Chile	20	28	77.9	146.1	99	4.3	19.5	0.10	11	56.8	-
	6	Loyalty	03	04	91.6	243.7	41	5.9	24.2	0.6	13	04.9	-

TABLE 3 (cont.)

Date		Location	O. h.	T m.	Δ deg.	Azimuth deg.	h km	M	C km/sec	rms error sec	T m.	T s.	dA/dΔ mμ/deg.
1965													
July	6	Greece	03	18	95.7	34.5	28	5.9	23.6	0.13	13	25.0	-
	6	Kurile	04	08	69.9	313.2	35	5.4	18.0	0.04	11	10.4	0.4
	6	Kamchatka	04	58	60.9	318.9	33	5.1	16.3	0.07	10	12.8	0.4
	6	Solomon	18	36	97.3	268.3	510	6.5	24.0	0.08	13	33.0	-3.0
	9	N. Atlantic	16	38	55.2	45.5	33	4.6	14.9	0.28	09	39.0	-
	12	Samoa	05	34	77.5	239.9	79	5.0	19.6	0.11	11	55.5	-
	12	Argentina	13	57	74.8	141.4	118	5.7	18.6	0.09	11	39.9	-
	13	Tonga	06	23	80.8	237.9	63	5.1	20.2	0.11	12	12.3	-
	13	Andreanoff	14	09	50.4	311.6	57	5.2	14.5	0.08	08	56.8	-
	14	Peru	12	29	65.7	135.6	143	5.1	16.9	0.15	10	44.4	-
	15	Santa Cruz	08	01	90.9	255.0	106	4.8	24.5	0.18	13	02.4	-
	15	E. Coast	14	16	29.8	73.5	0	5.1	12.8	0.16	06	07.0	-
	19	Fiji	23	53	90.0	237.5	482	6.0	24.2	0.09	12	58.5	-0.7
	20	Kurile	11	19	66.9	314.1	4	5.4	17.2	0.07	10	52.9	-
	20	Fox	20	11	43.4	314.5	87	5.3	13.7	0.14	08	01.7	-1.1
	25	Japan	13	33	76.3	310.7	33	5.9	19.3	0.07	11	48.3	-

FIGURE CAPTIONS

Figure 1. Filtering operations in frequency-wavenumber space.

Figure 2. Frequency response of the nonlinear filter for a one-cycle sine wave of period Q. W is the filter length.

Figure 3. Pulse distortion as a function of the correlation window T. The filter window W equals T/2 in all cases.

Figure 4. Amplitude response as a function of the correlation window T for a pulse of duration 2Q. The filter window W equals T/2 in all cases.

Figure 5. Amplitude response as a function of the filter window W. The correlation window T is equal to 4, which is the pulse duration, in all cases.

Figure 6. Pulse distortion as a function of the filter window W. The correlation window T is constant and equal to the pulse duration.

Figure 7. The effect of noise on the nonlinear filter.

Figure 8. Site locations for the extended array at TFSO.

Figure 9. Instrument response for the extended array at TFSO.

Figure 10. Wavenumber response for the summation of the extended array at TFSO.

Figure 11. Crustal structure and Bouguer gravity anomalies along the NE-SW leg of the extended array at TFSO.

Figure 12. Geometry used for computing crustal corrections.

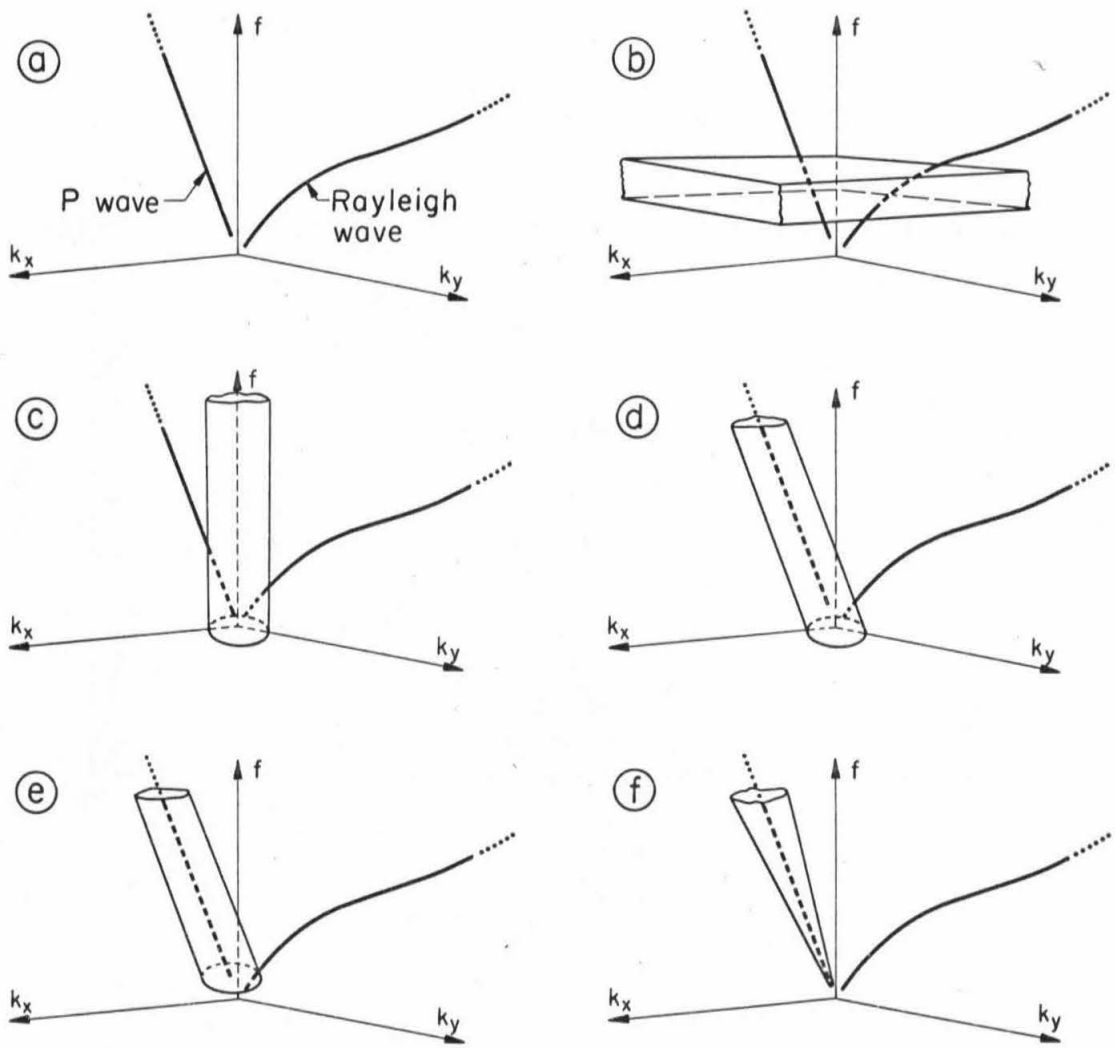
a
f
P wave
Rayleigh wave
k_x
k_y
b
f
k_x
k_y
c
f
k_x
k_y
d
f
k_x
k_y
e
f
k_x
k_y
f
f
k_x
k_y

Fig. 1

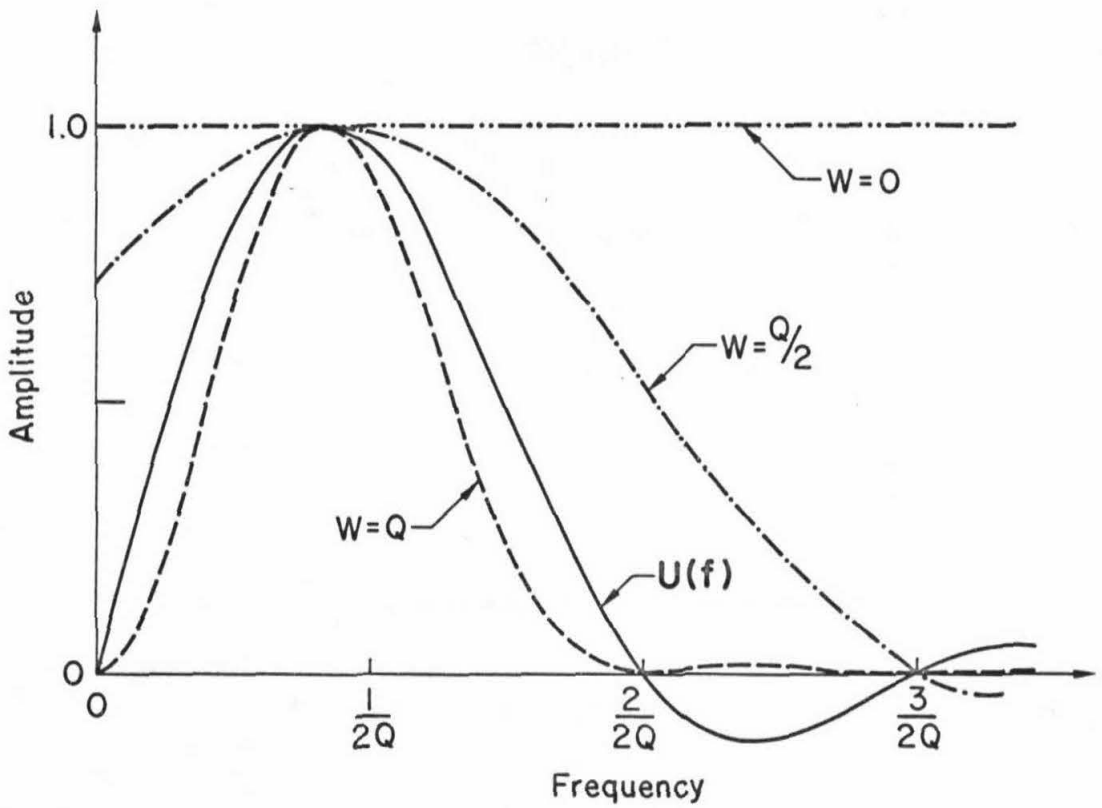

Fig. 2

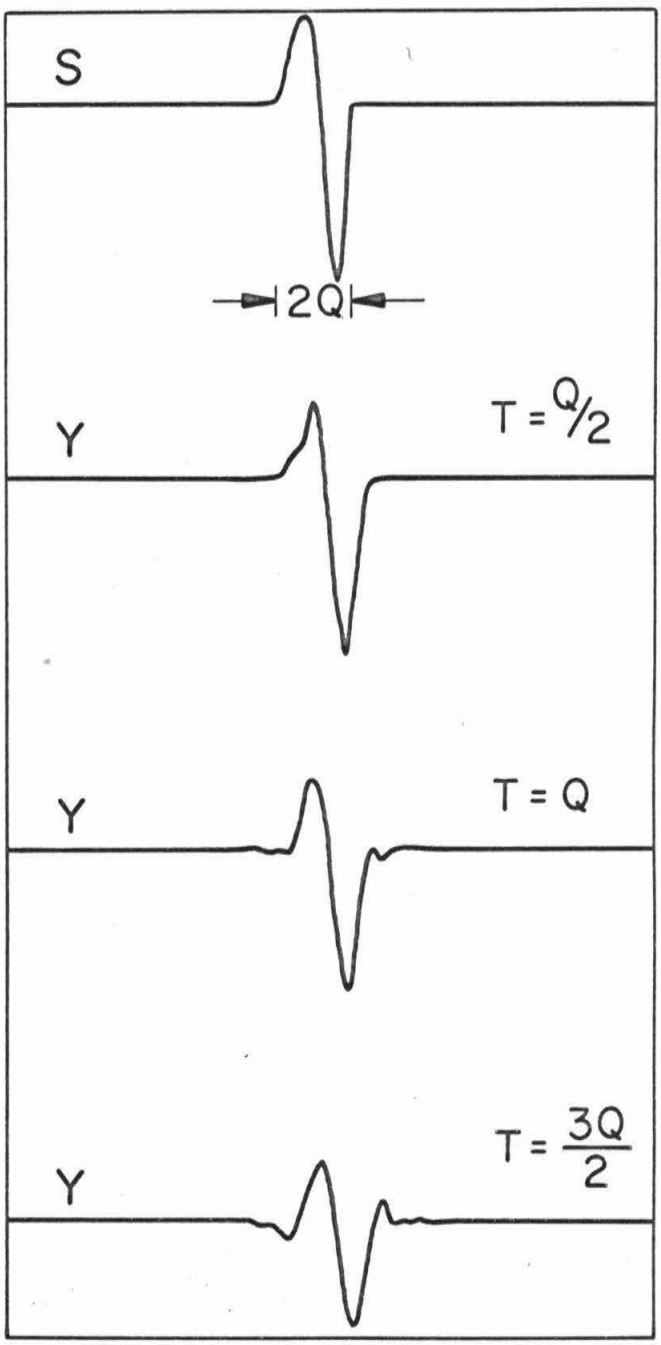

Fig. 3

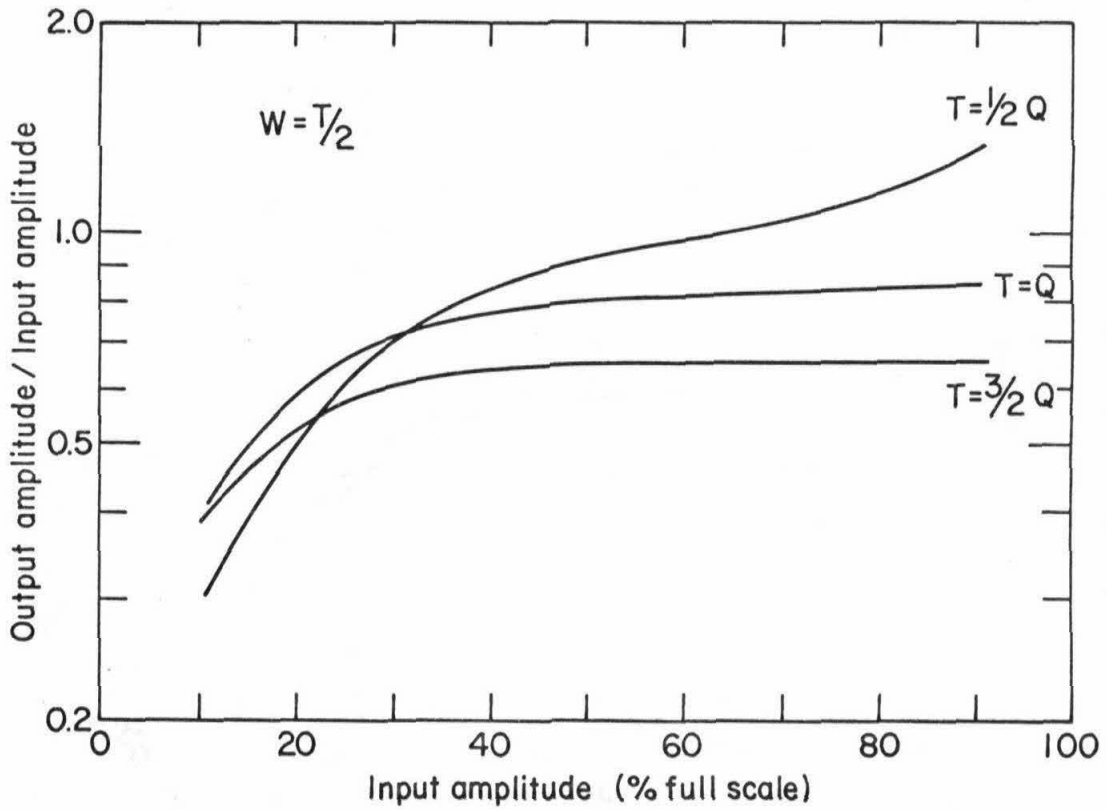
2.0
1.0
0.5
0.2
0
20
40
60
80
100
W = T/2
T=½ Q
T=Q
T=3/2 Q
Output amplitude / Input amplitude
Input amplitude (% full scale)

Fig. 4

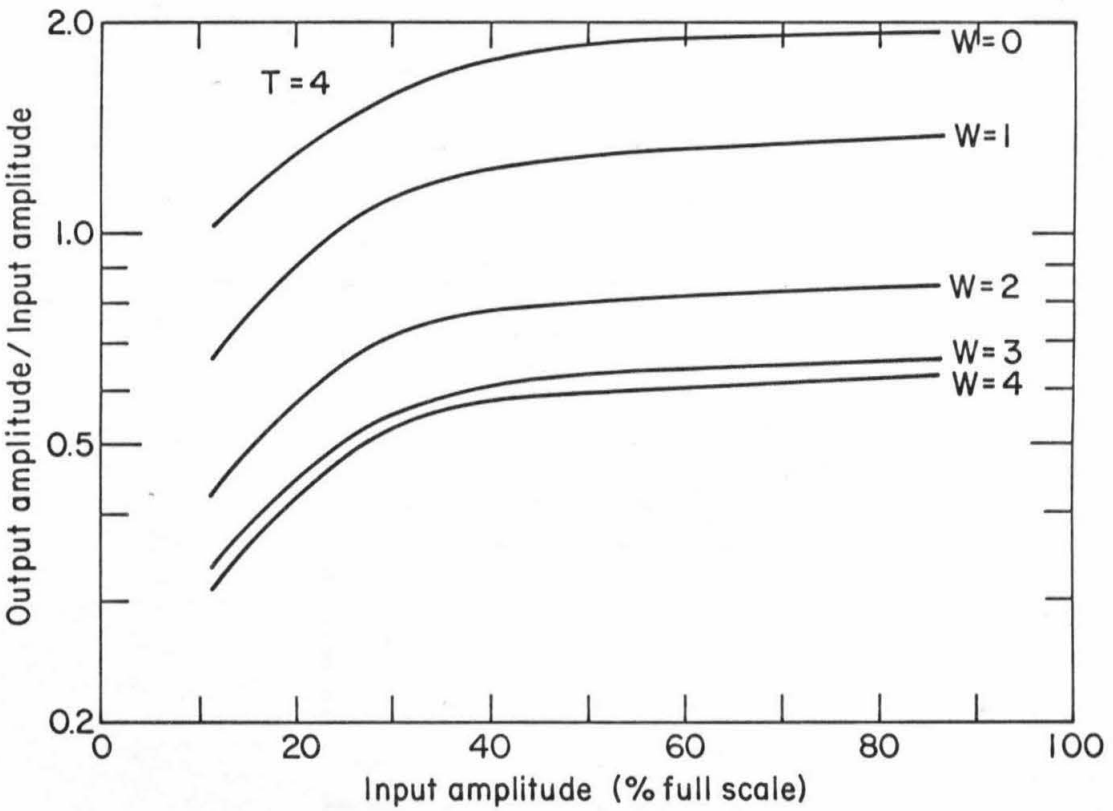
2.0
1.0
0.5
0.2
0
20
40
60
80
100
T = 4
W = 0
W = 1
W = 2
W = 3
W = 4
Output amplitude / Input amplitude
Input amplitude (% full scale)

Fig. 5

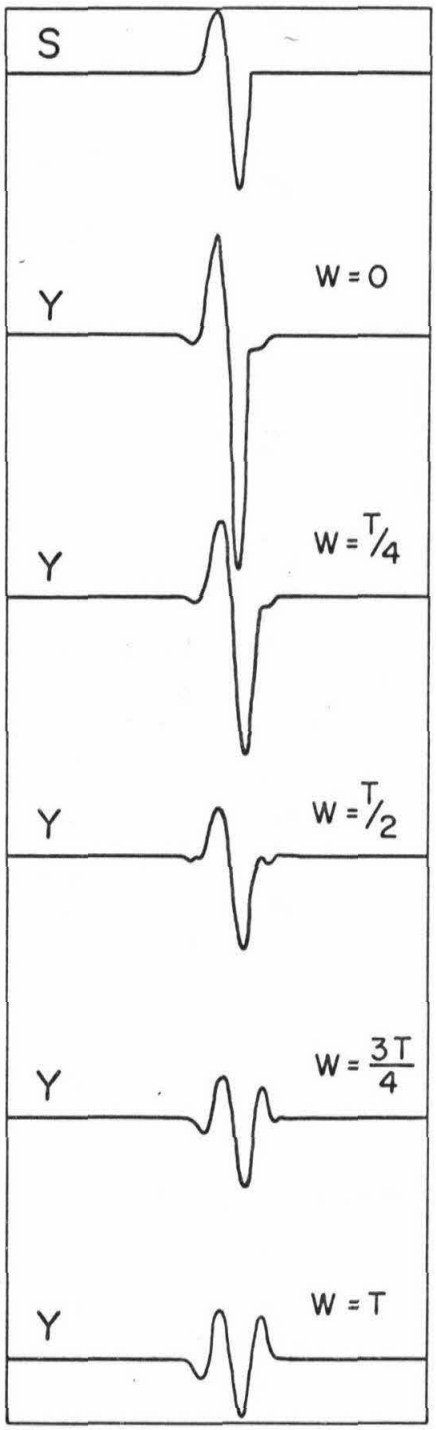

Fig. 6

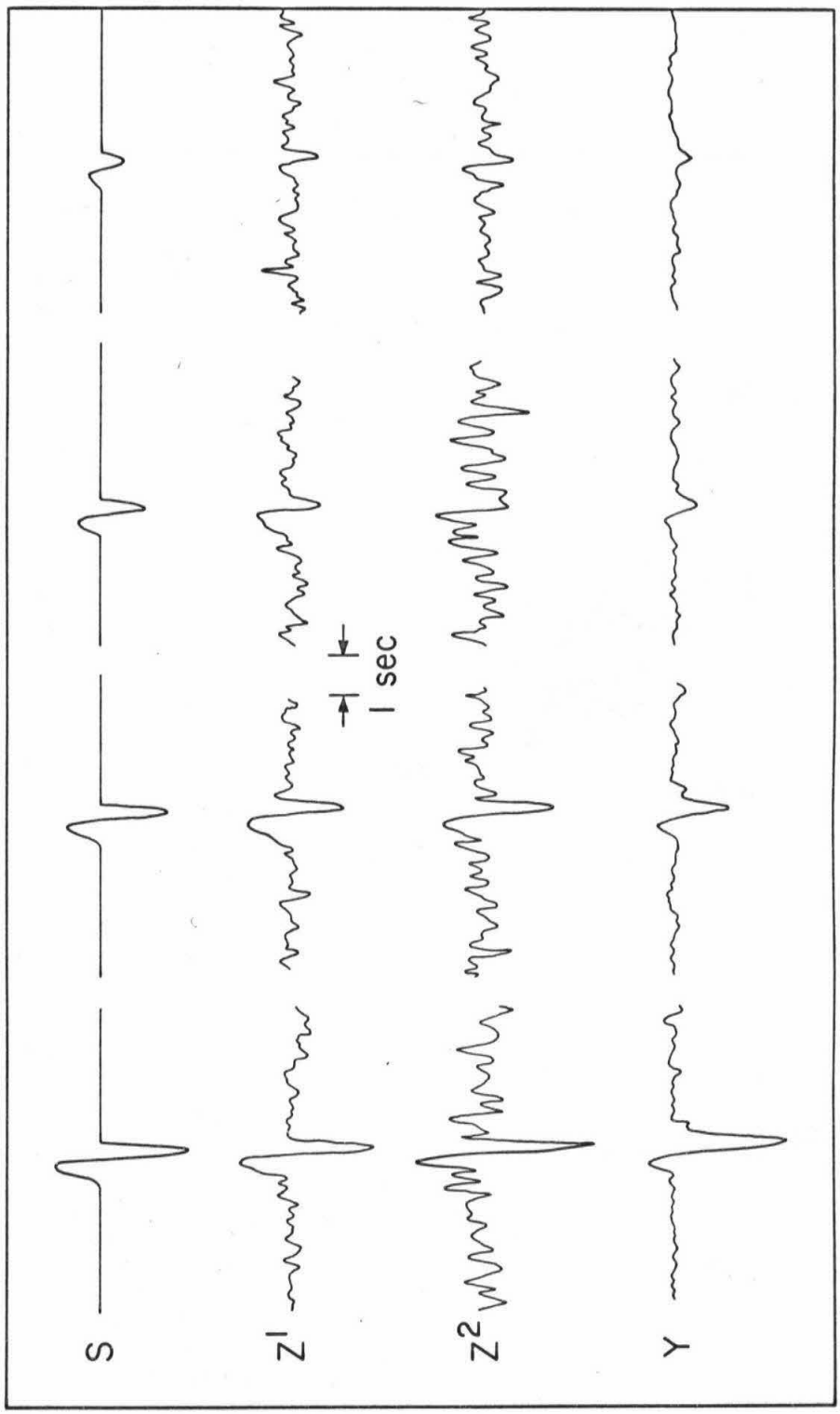

Fig. 7

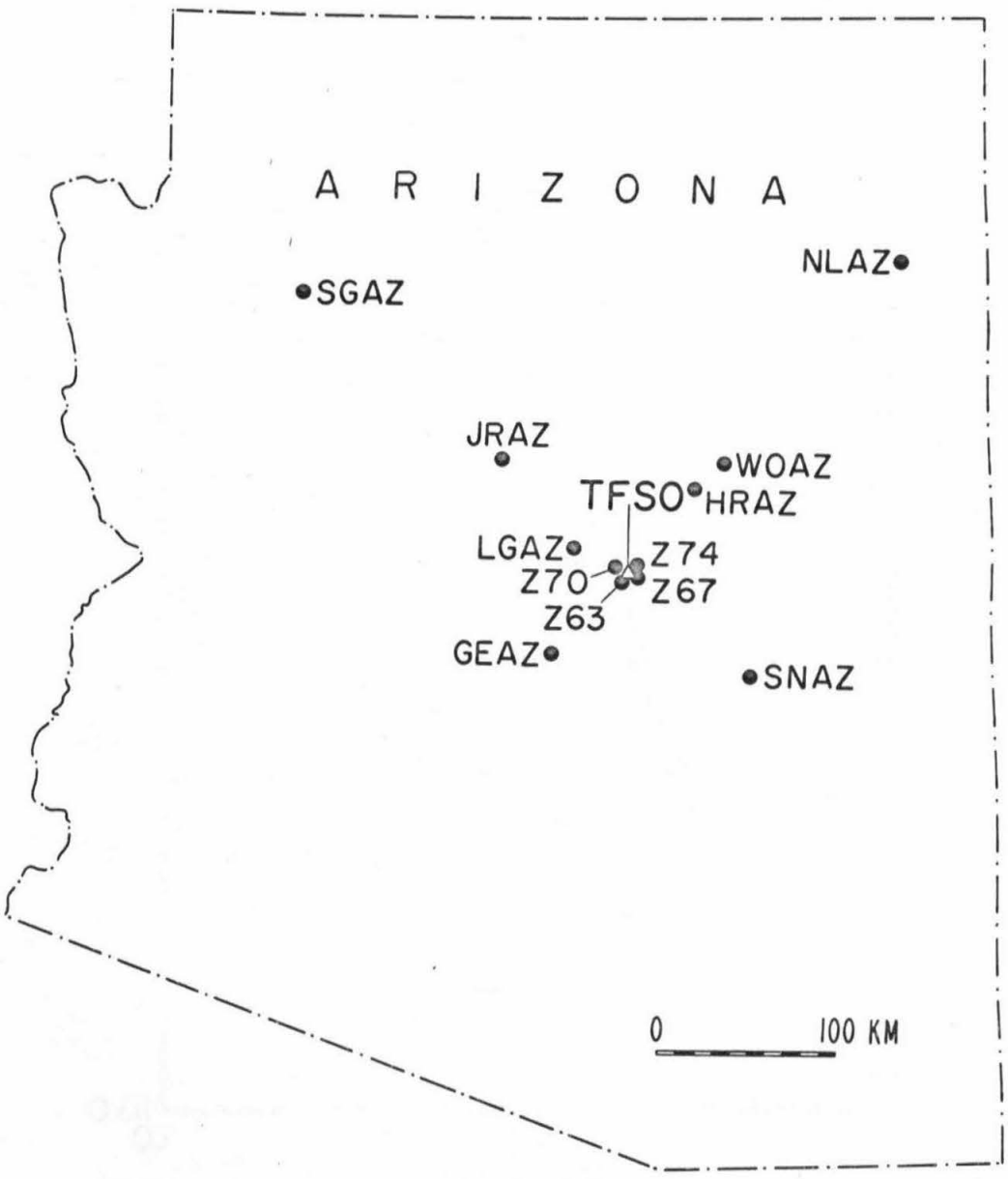
A R I Z O N A
NLAZ
SGAZ
JRAZ
WOAZ
TFSO
HRAZ
LGAZ
Z74
Z70
Z67
Z63
GEAZ
SNAZ
0
100 KM

Fig. 8

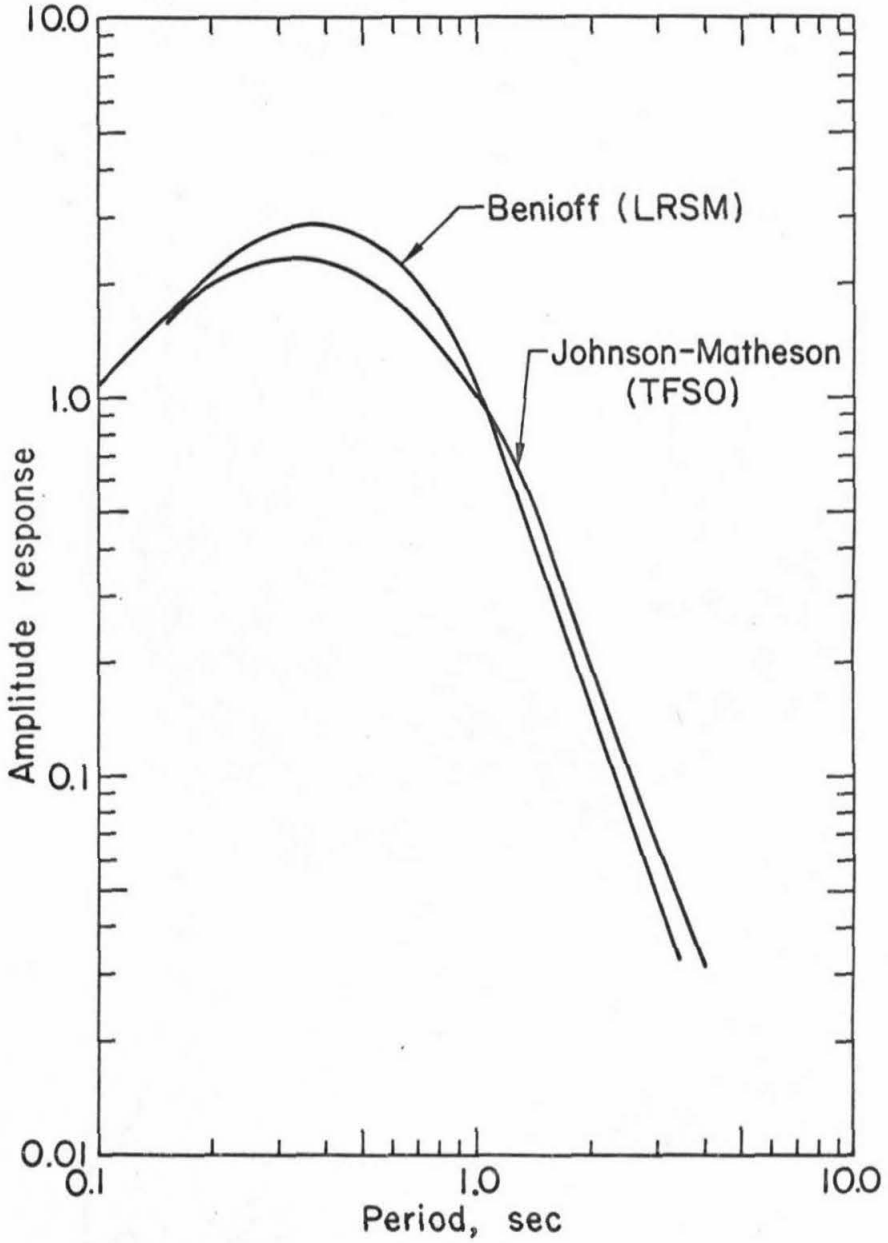
10.0
1.0
0.1
0.01
0.1
1.0
10.0
Amplitude response
Period, sec
Benioff (LRSM)
Johnson-Matheson
(TFSO)

Fig. 9

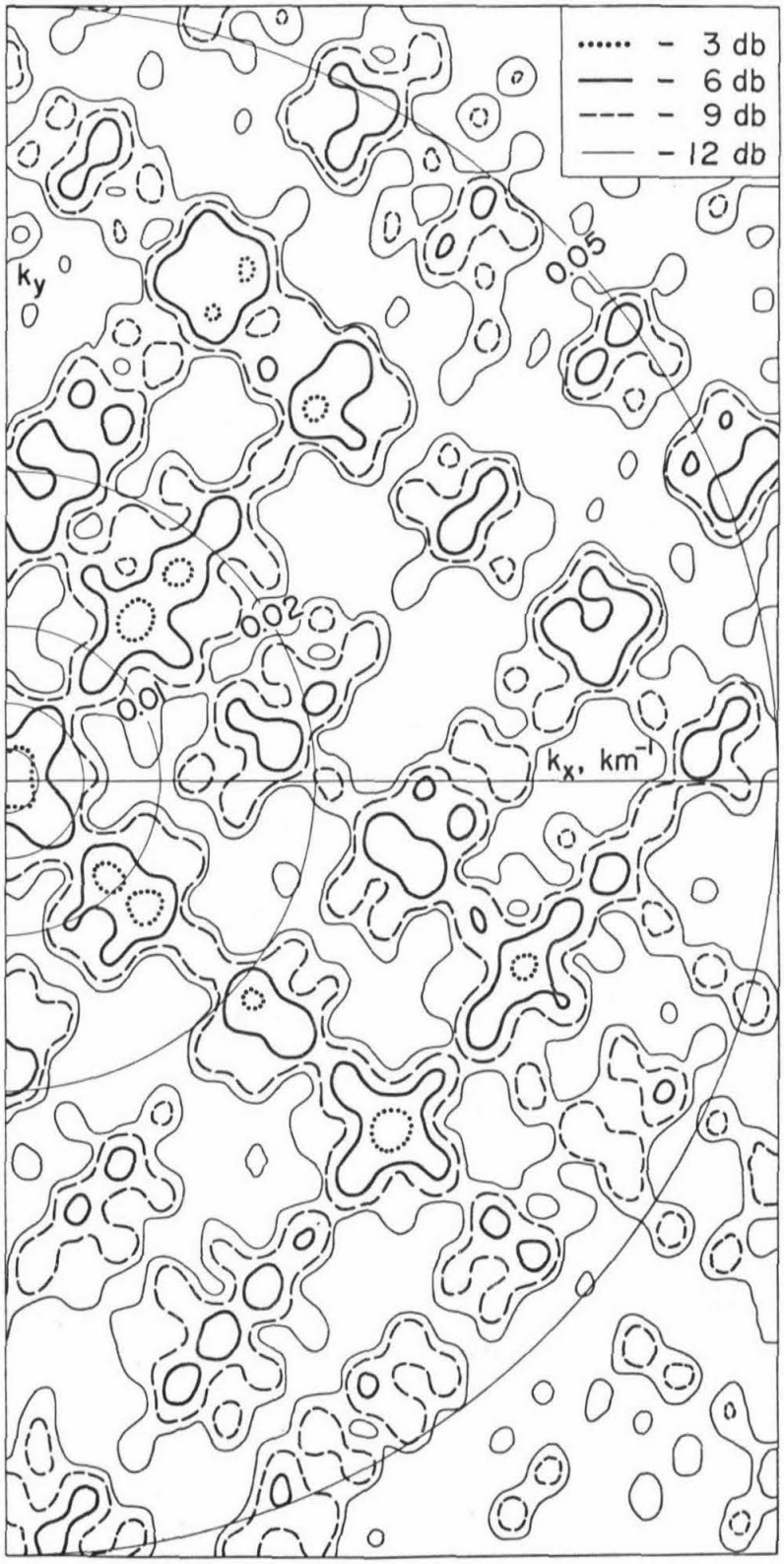

Fig. 10

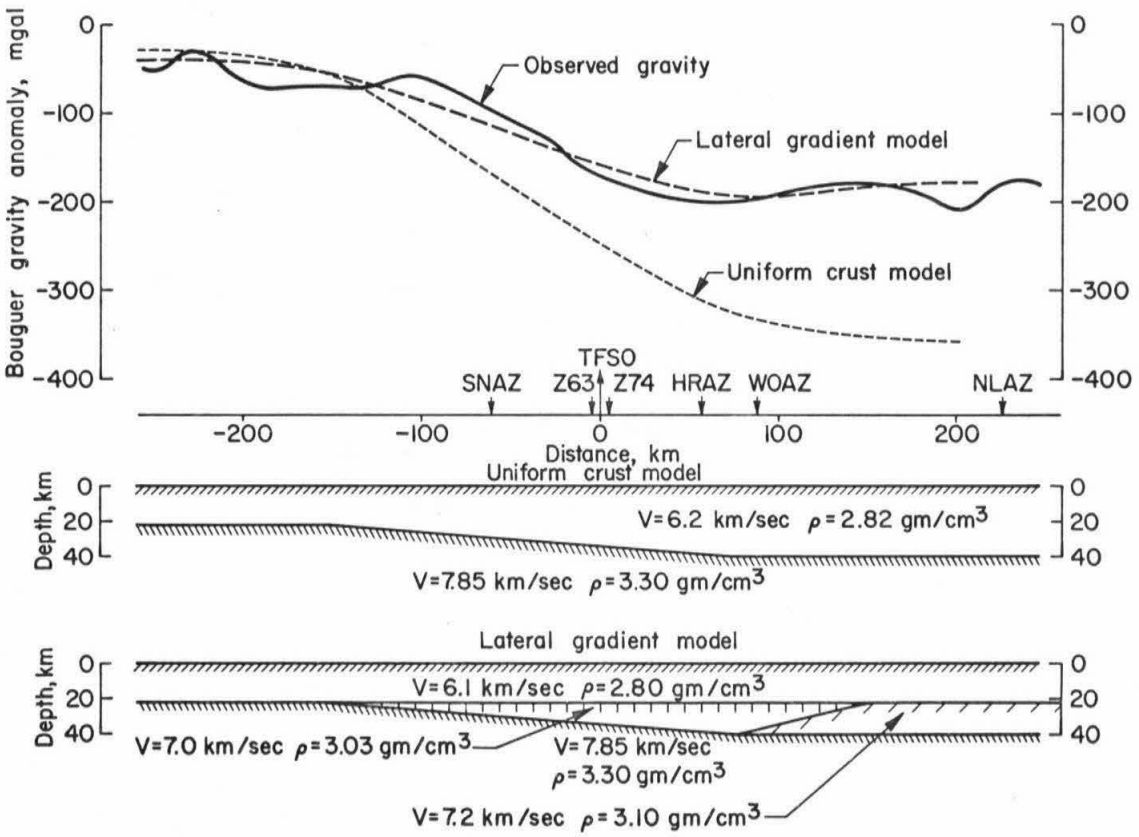
Bouguer gravity anomaly, mgal
0
-100
-200
-300
-400
Observed gravity
Lateral gradient model
Uniform crust model
TFSO
SNAZ
Z63
Z74
HRAZ
WOAZ
NLAZ
-200
-100
0
100
200
Distance, km
Uniform crust model
Depth, km
0
20
40
V=6.2 km/sec ρ=2.82 gm/cm3
V=7.85 km/sec ρ=3.30 gm/cm3
Lateral gradient model
V=6.1 km/sec ρ=2.80 gm/cm3
V=7.0 km/sec ρ=3.03 gm/cm3
V=7.85 km/sec
ρ=3.30 gm/cm3
V=7.2 km/sec ρ=3.10 gm/cm3

Fig. 11

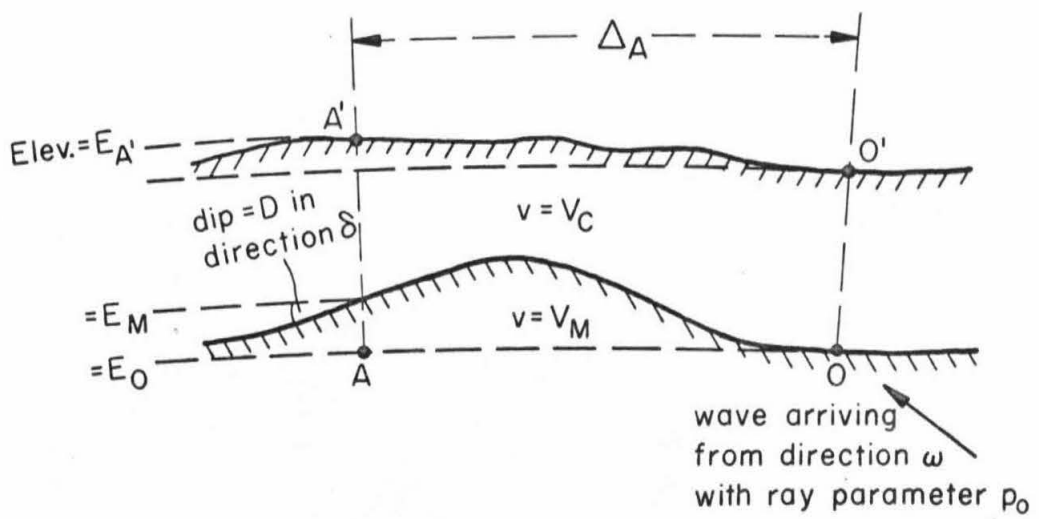
Δ_A
A'
O'
Elev.=$E_{A'}$
dip = D in direction δ
v = V_C
=E_M
v = V_M
=E_O
A
O
wave arriving from direction ω with ray parameter p_o

Fig. 12

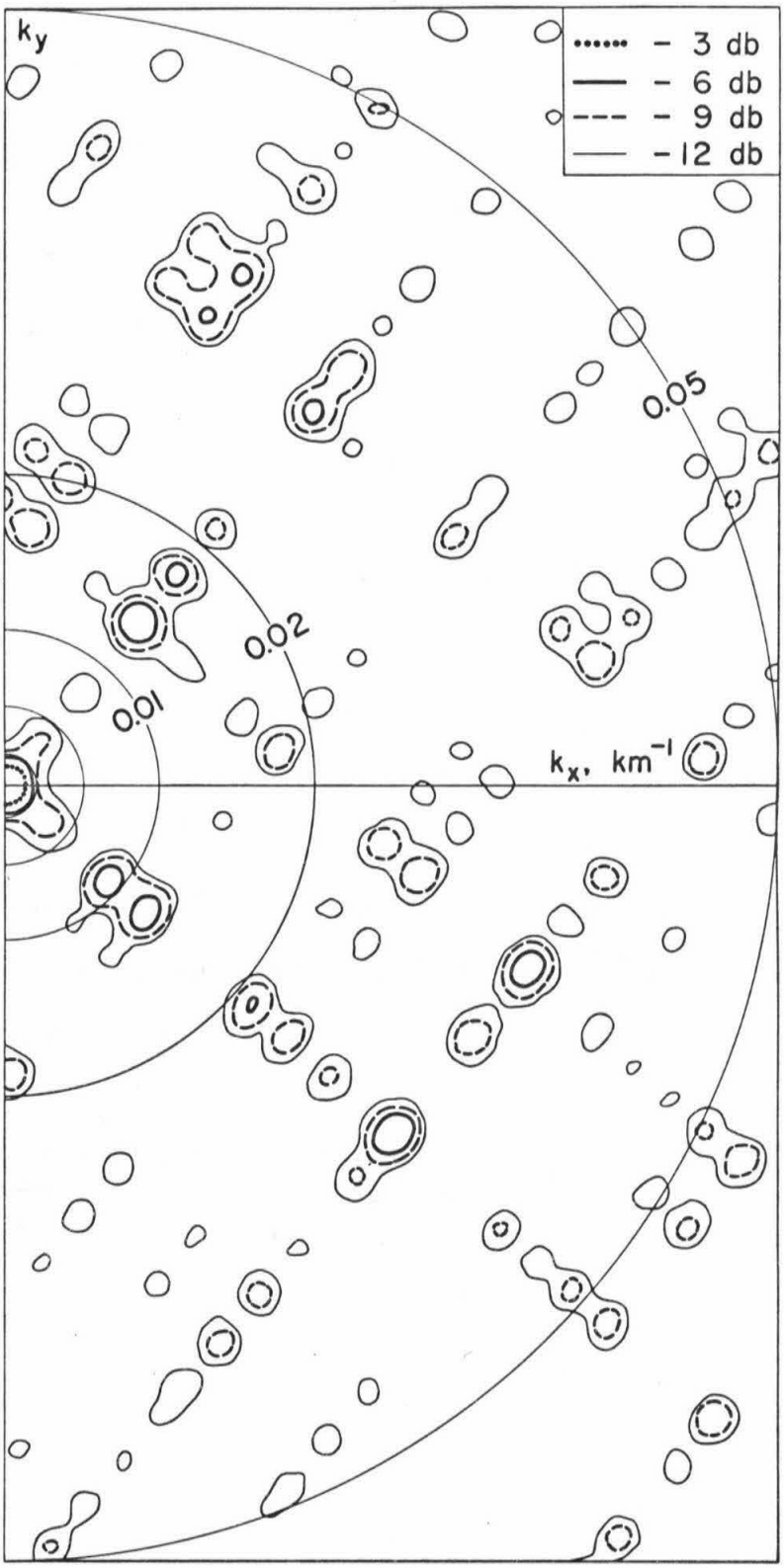

Fig. 13

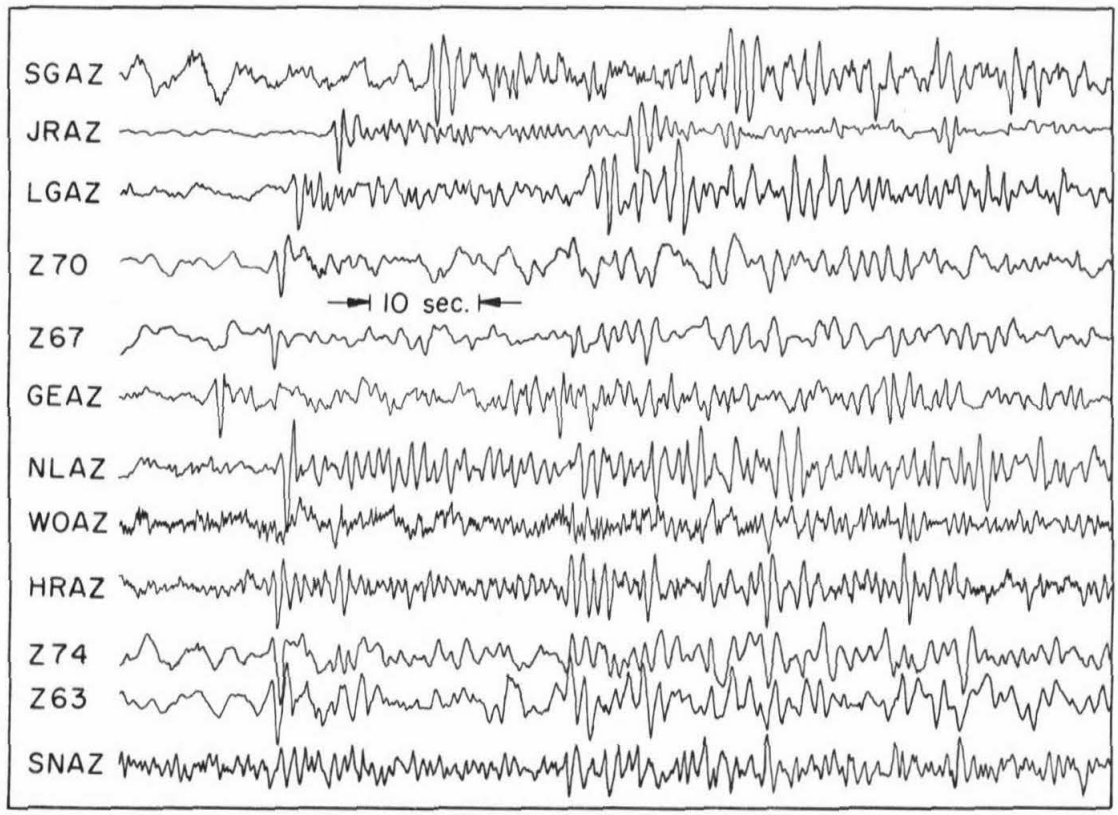

Fig. 14

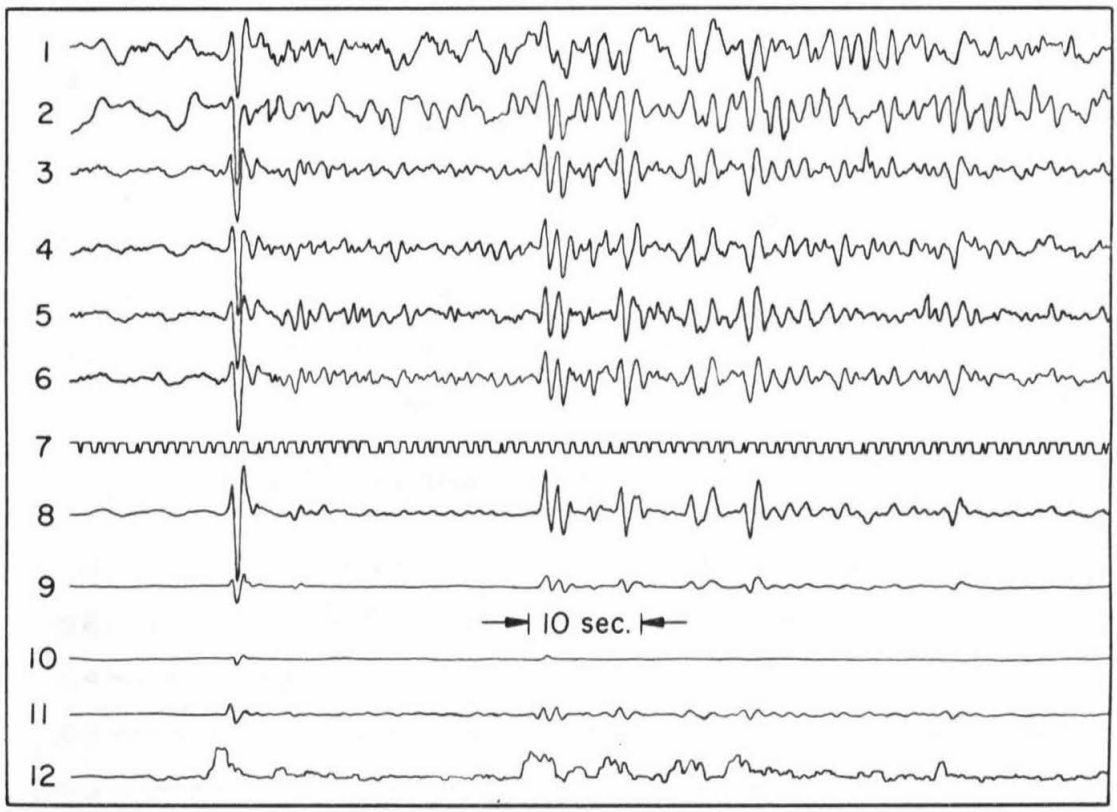

Fig. 15

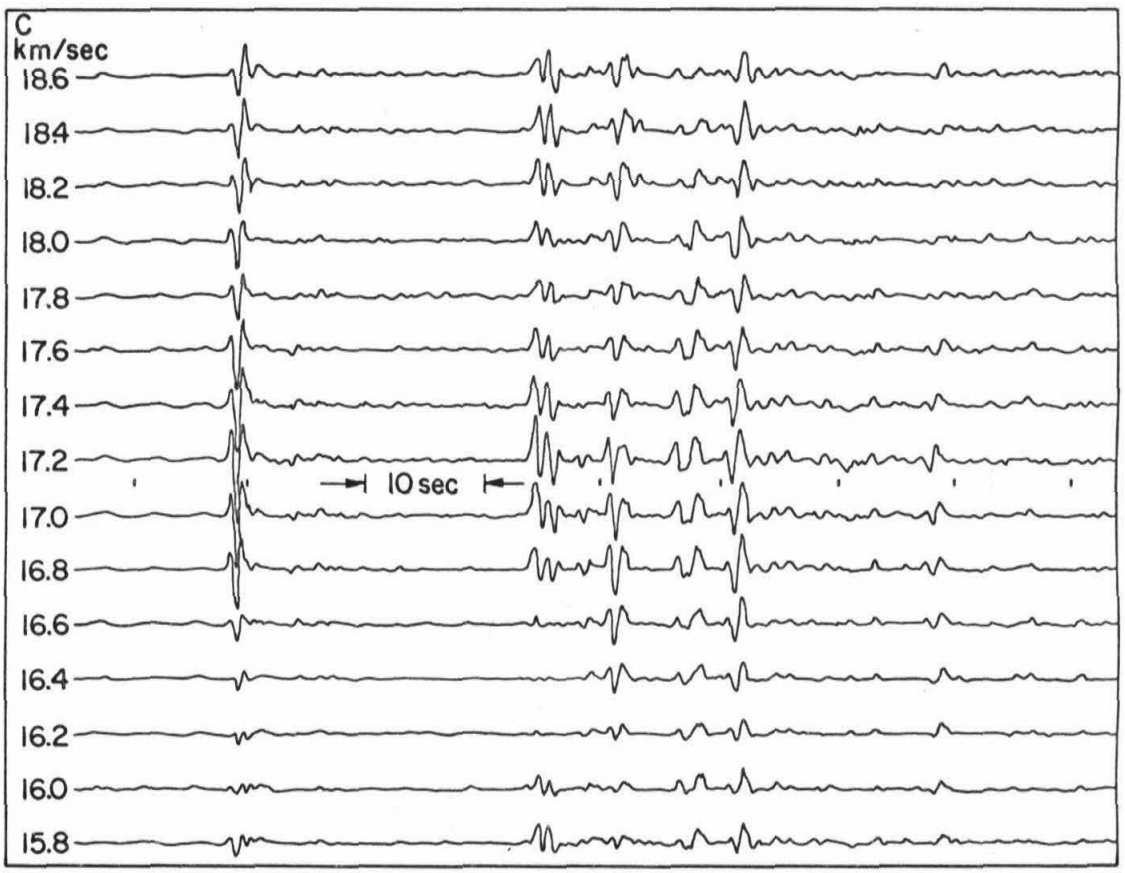
C
km/sec
18.6
18.4
18.2
18.0
17.8
17.6
17.4
17.2
10 sec
17.0
16.8
16.6
16.4
16.2
16.0
15.8

Fig. 16

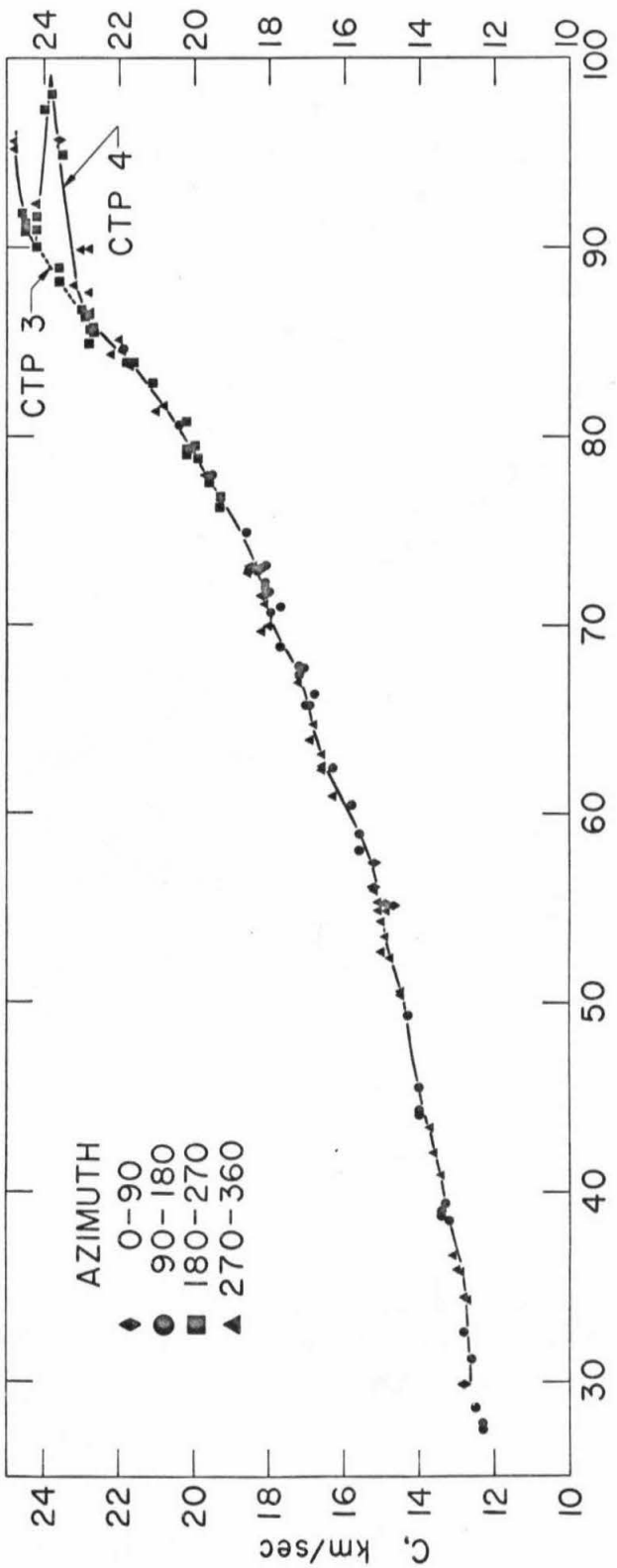
AZIMUTH
0-90
90-180
180-270
270-360
CTP 3
CTP 4
c, km/sec
Δ, deg.
10
12
14
16
18
20
22
24
30
40
50
60
70
80
90
100

Fig. 17

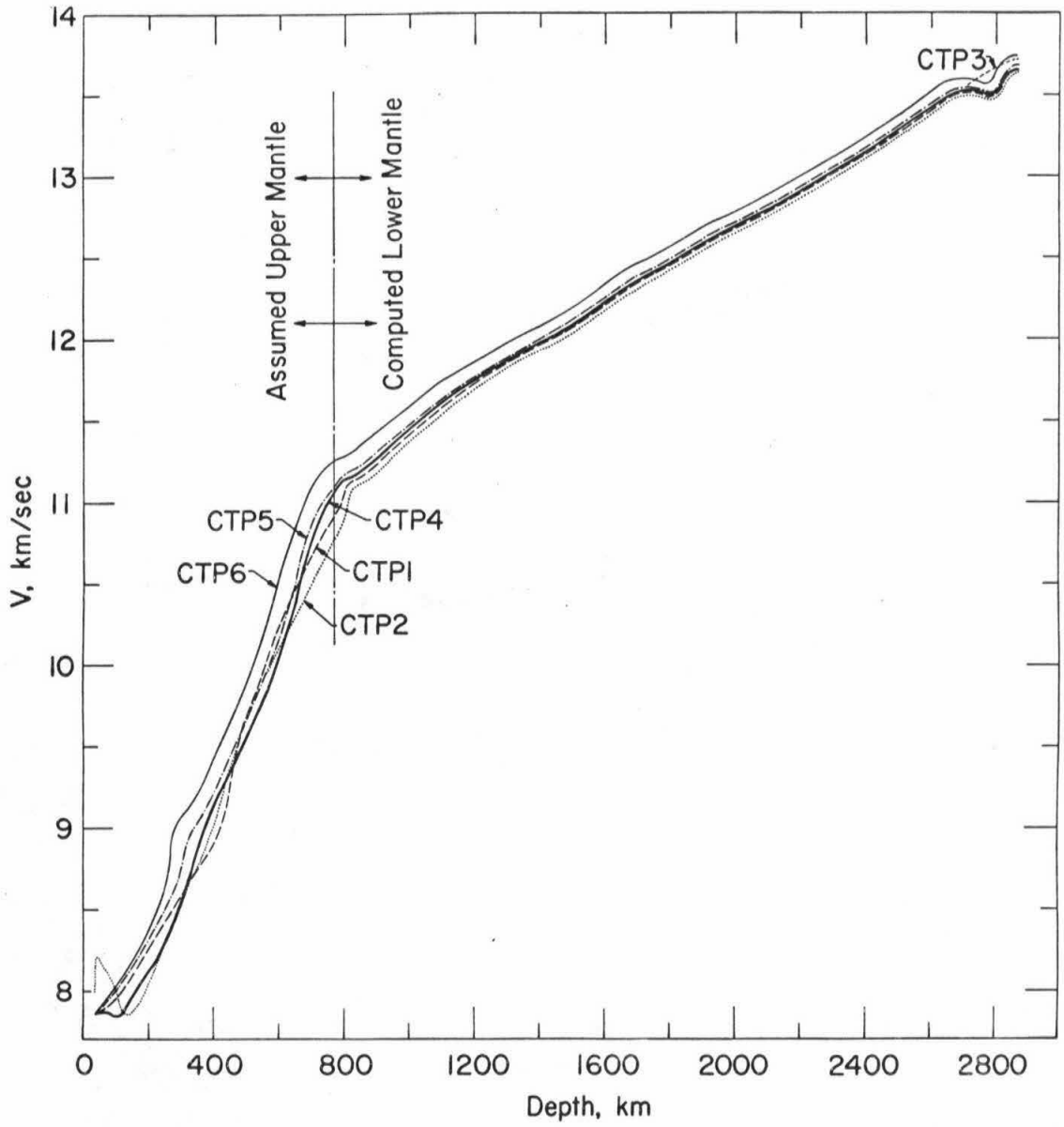
14
13
12
11
10
9
8
V, km/sec
0
400
800
1200
1600
2000
2400
2800
Depth, km
Assumed Upper Mantle
Computed Lower Mantle
CTP3
CTP5
CTP4
CTP6
CTPI
CTP2

Fig. 18

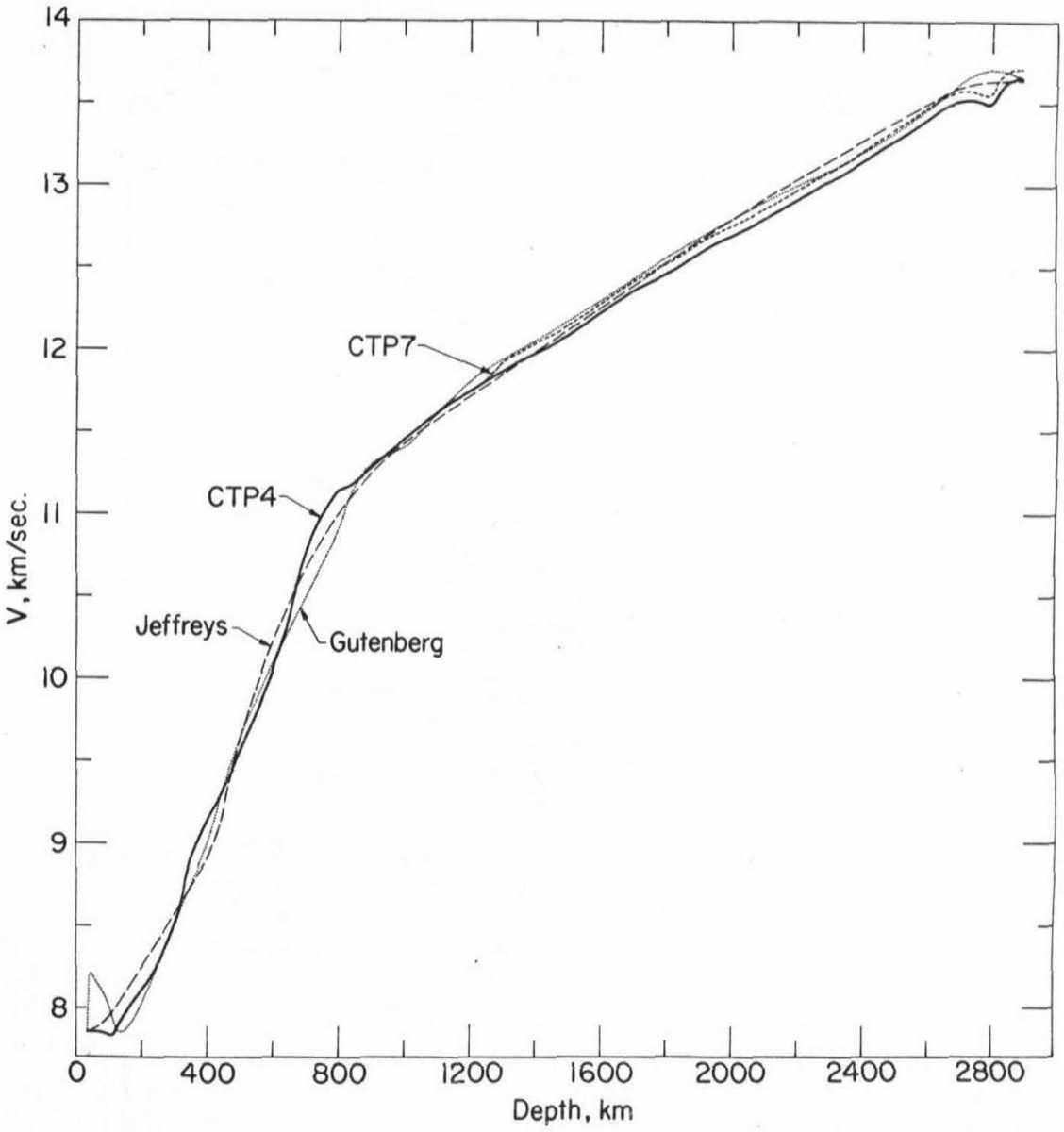
14
13
12
11
10
9
8
V, km/sec.
CTP7
CTP4
Jeffreys
Gutenberg
0
400
800
1200
1600
2000
2400
2800
Depth, km

Fig. 19

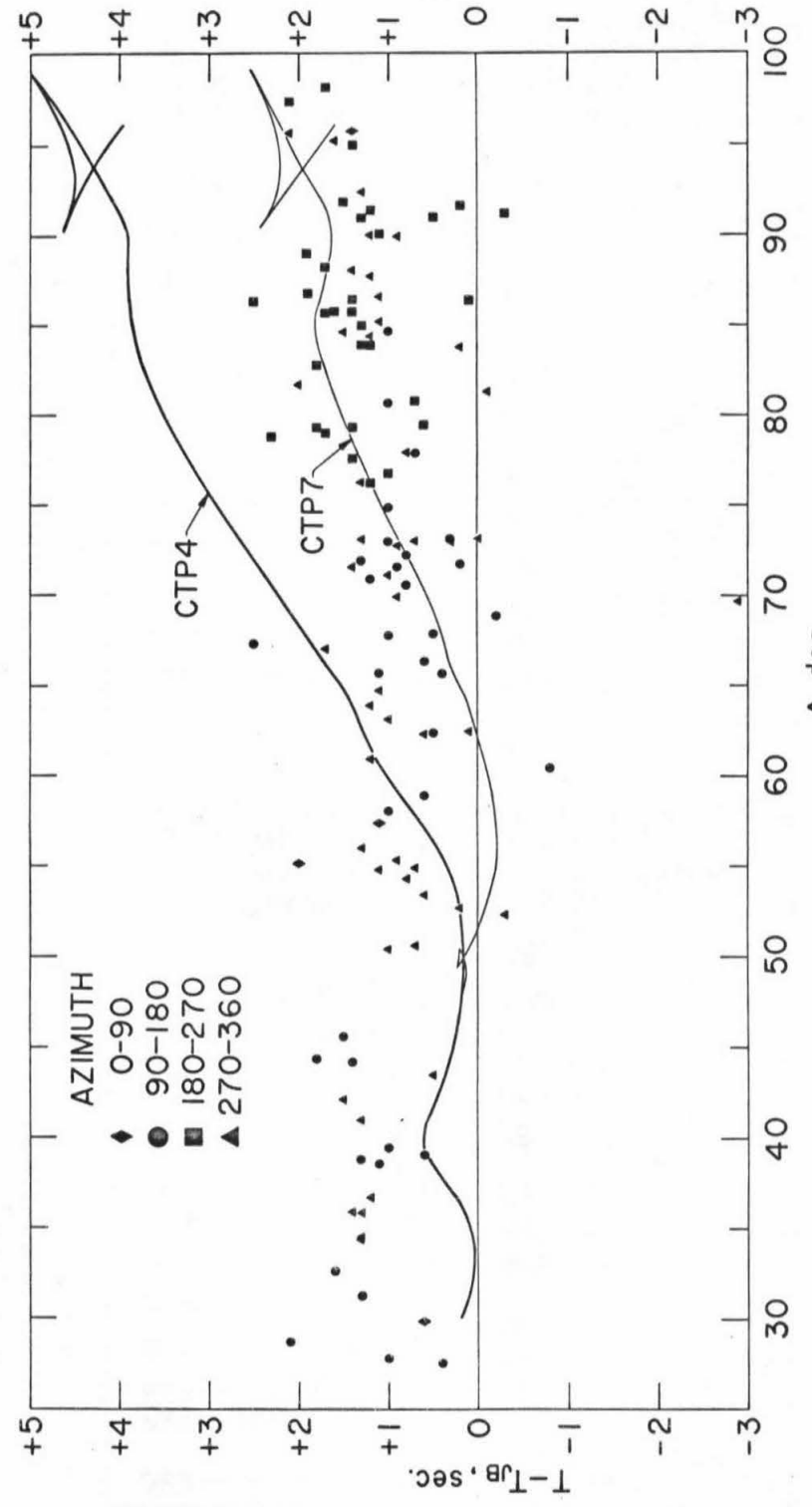
AZIMUTH
0-90
90-180
180-270
270-360
CTP4
CTP7
T−TJB, sec.
Δ, deg.
+5
+4
+3
+2
+1
0
-1
-2
-3
30
40
50
60
70
80
90
100

Fig. 20

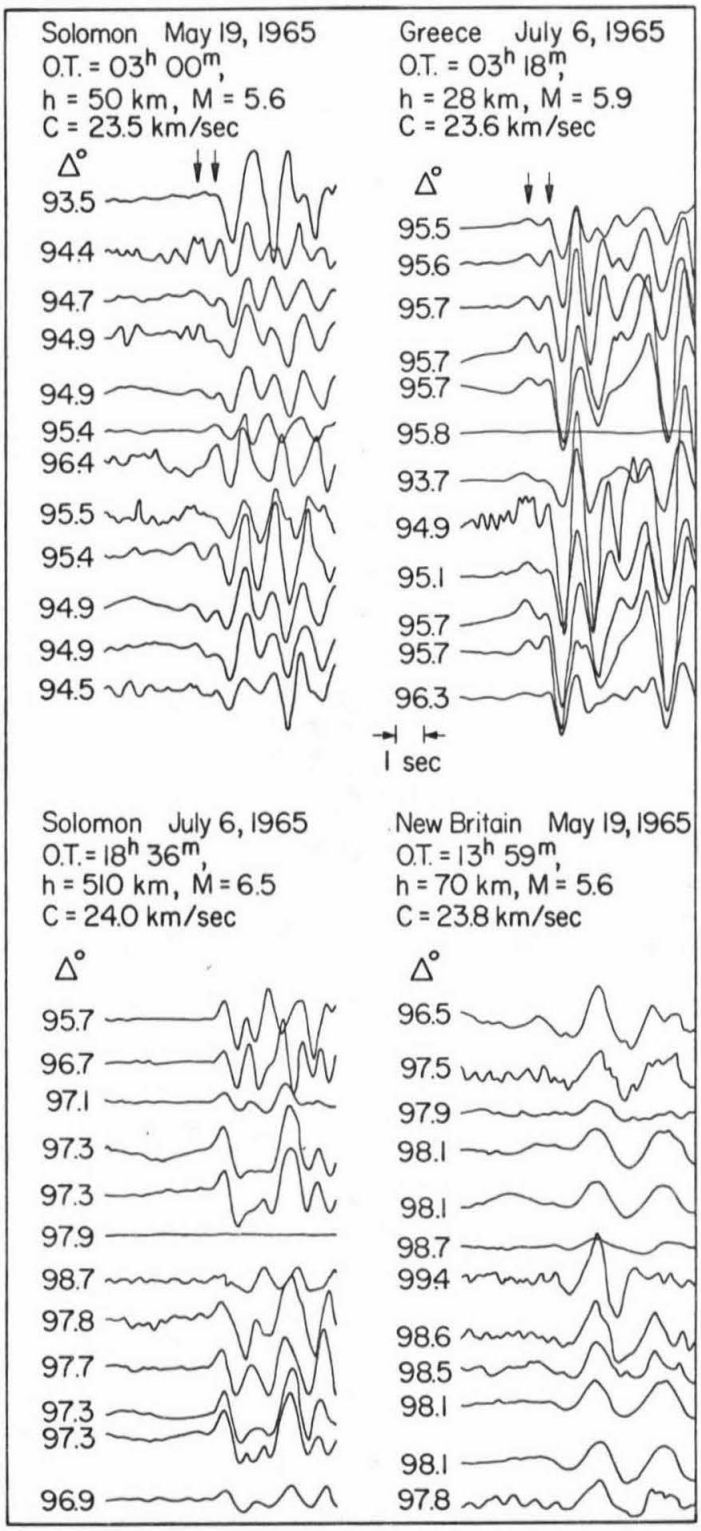
Solomon May 19, 1965
O.T. = 03h 00m,
h = 50 km, M = 5.6
C = 23.5 km/sec
Δ°
93.5
94.4
94.7
94.9
94.9
95.4
96.4
95.5
95.4
94.9
94.9
94.5
Greece July 6, 1965
O.T. = 03h 18m,
h = 28 km, M = 5.9
C = 23.6 km/sec
Δ°
95.5
95.6
95.7
95.7
95.7
95.8
93.7
94.9
95.1
95.7
95.7
96.3
1 sec
Solomon July 6, 1965
O.T. = 18h 36m,
h = 510 km, M = 6.5
C = 24.0 km/sec
Δ°
95.7
96.7
97.1
97.3
97.3
97.9
98.7
97.8
97.7
97.3
97.3
96.9
New Britain May 19, 1965
O.T. = 13h 59m,
h = 70 km, M = 5.6
C = 23.8 km/sec
Δ°
96.5
97.5
97.9
98.1
98.1
98.7
99.4
98.6
98.5
98.1
98.1
97.8

Fig. 21

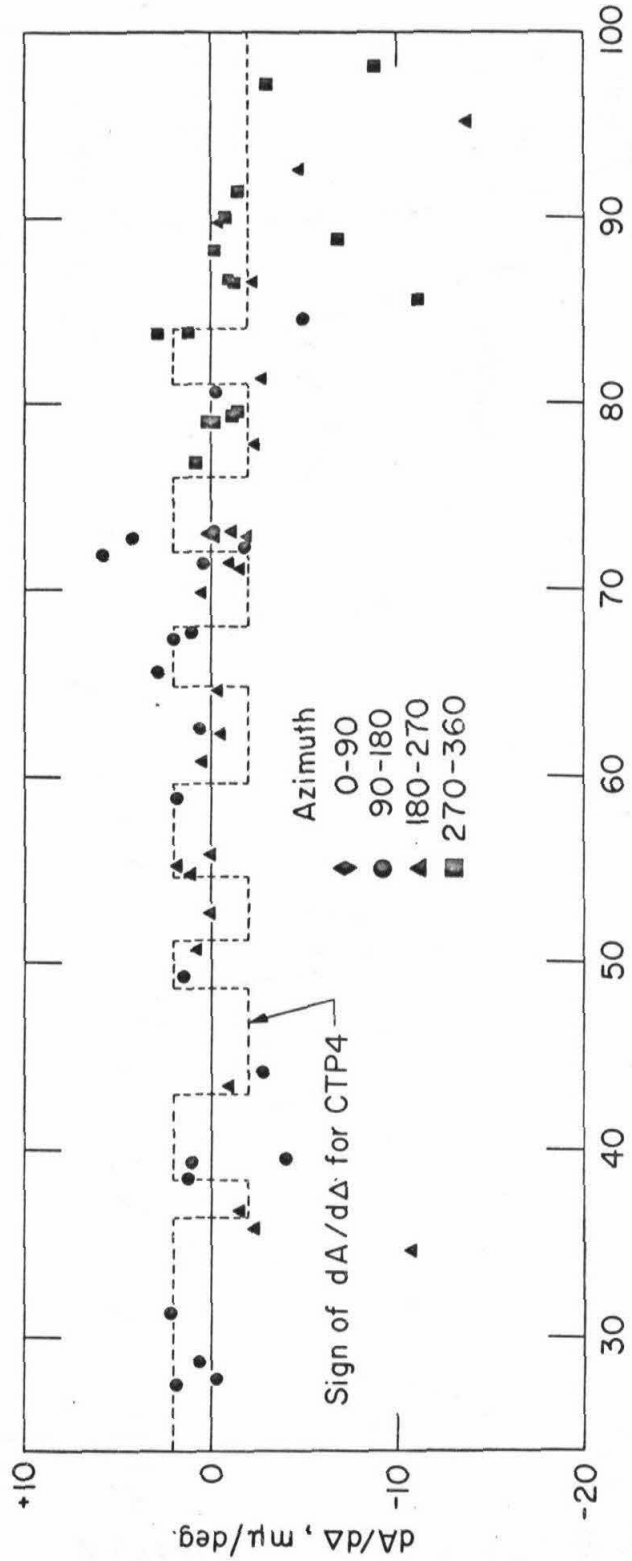
+10
0
-10
-20
dA/dΔ , mμ/deg.
30
40
50
60
70
80
90
100
Δ, deg.
Azimuth
0-90
90-180
180-270
270-360
Sign of dA/dΔ for CTP4

Fig. 22

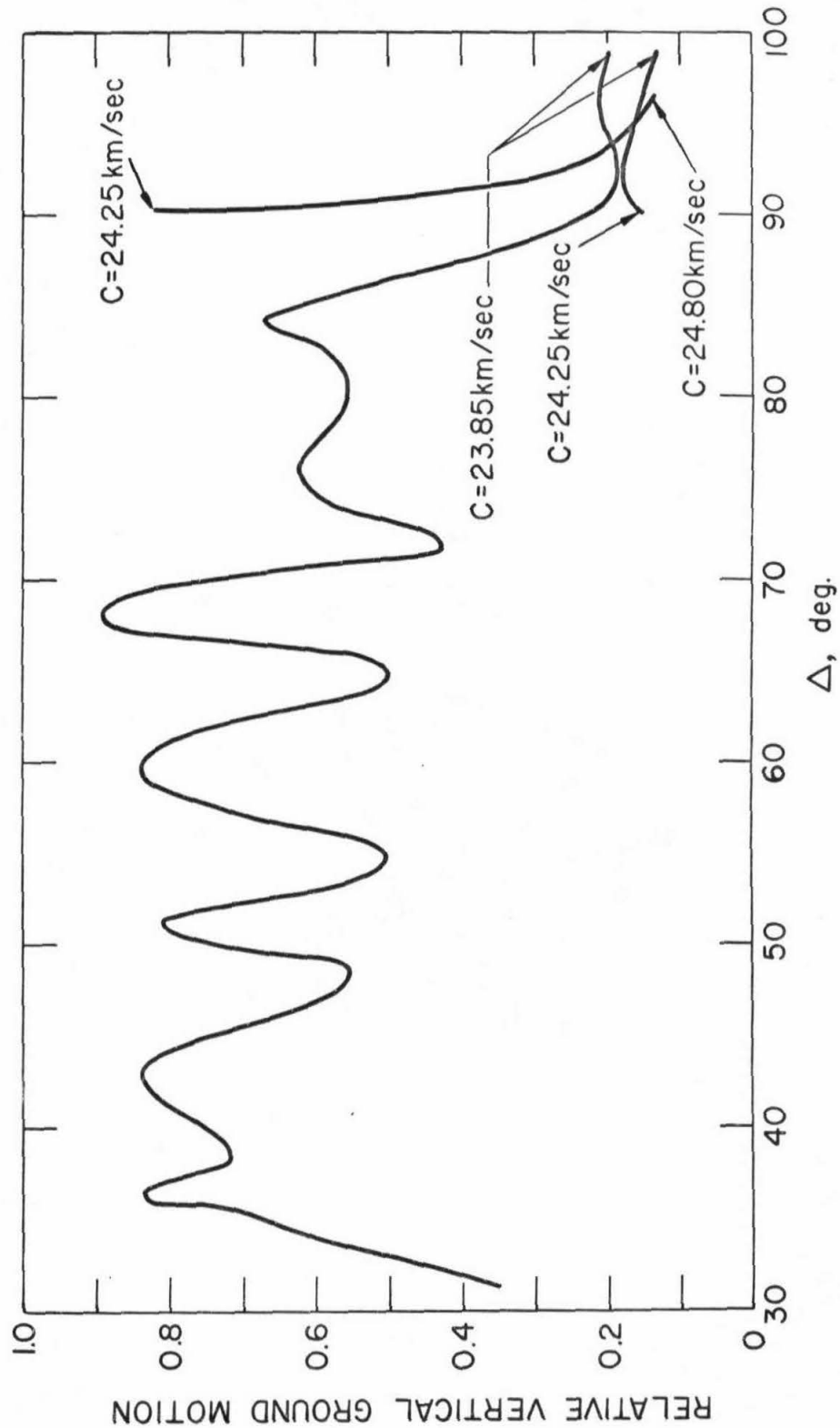
C=24.25km/sec
C=23.85km/sec
C=24.25km/sec
C=24.80km/sec
RELATIVE VERTICAL GROUND MOTION
0
0.2
0.4
0.6
0.8
1.0
30
40
50
60
70
80
90
100
Δ, deg.

Fig. 23

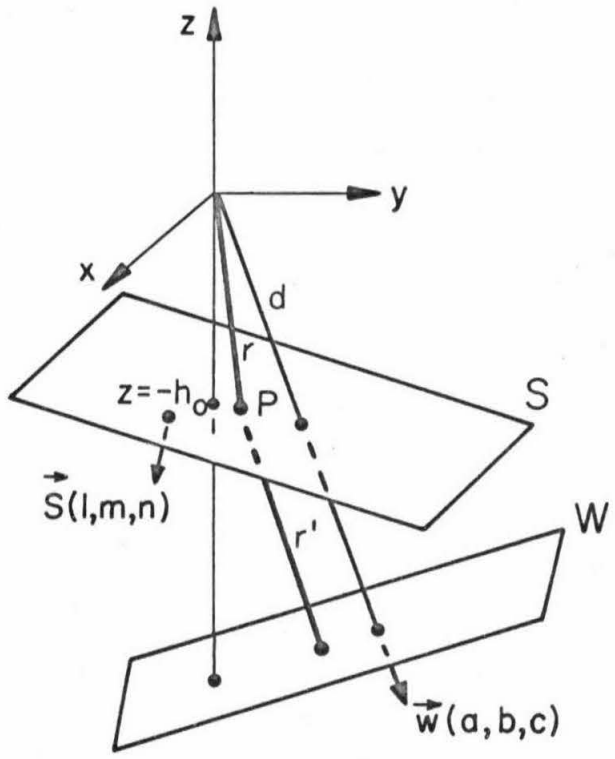

Fig. 24